Materials Science and Engineering

Second cycle, 30 credits

MH202X

Characterization of Conductive Surface Treatments for TRATON Battery Enclosure Lids

Balancing corrosion protection with electrical conductivity and automotive durability

Ajai Krishna

KTH Royal Institute of Technology

Characterization of Conductive Surface Treatments for TRATON Battery Enclosure Lids

Balancing corrosion protection with electrical conductivity and automotive durability

Ajai Krishna

Degree project in Materials Science and Engineering
Degree Project in Materials and Process Design, Second Cycle
Second cycle, 30 credits
MH202X

TRATON supervisor: Raghda Kalifa
RISE supervisor: Johan Tidblad
KTH mentor: Christopher Hulme

Examiner: Christopher Hulme

Commissioning organisation: TRATON

Stockholm, September 14, 2026

Abstract

This thesis investigates conductive surface treatments for battery enclosure lids used in electrified heavy vehicles. The work was carried out at TRATON in collaboration with RISE. Alternative surface-treatment systems are compared with the current reference system, with emphasis on the balance between electrical conductivity, corrosion resistance, adhesion, mechanical durability, environmental aging resistance, and chemical resistance.

The experimental work comprised coating thickness measurement, adhesion evaluations after different conditioning routes, chemical resistance testing, UV/weathering exposure, two accelerated cyclic corrosion routes, microscopy with SEM/EDS support, constrained mechanical characterization, DSC thermal analysis of powder coatings, and comparative dry-circuit electrical resistance measurement. *Series 22* gave the lowest measured resistance and was the strongest conductive candidate, although local red-corrosion observations in ACT1 require further corrosion-risk control. *Series 24* remained the protective reference but behaved as an electrical insulator in the coupon screening, whereas *Series 27* achieved the cleanest powder-coated ACT1 outcome without providing measurable conductivity. The results demonstrate that coating selection must balance electrical function with corrosion protection and mechanical and environmental durability rather than maximize conductivity alone.

Keywords
conductive surface treatment, battery enclosure, corrosion resistance, electrical conductivity, automotive durability

Sammanfattning

Examensarbetet undersöker ledande ytbehandlingssystem för lock till batteriinneslutningar i elektrifierade tunga fordon. Arbetet genomfördes vid TRATON i samarbete med RISE och jämför alternativa ytbehandlingssystem med det nuvarande referenssystemet.

Fokus ligger på avvägningen mellan elektrisk ledningsförmåga, korrosionsskydd, vidhäftning, mekanisk hållbarhet, beständighet mot miljöåldring och kemikalier. Det experimentella arbetet omfattade tjockleksmätning, vidhäftningsprovning, kemikaliebeständighet, UV- och väderbeständighet, två accelererade cykliska korrosionsprovningar, mikroskopi med SEM/EDS, mekanisk karakterisering, DSC-analys och jämförande elektrisk resistansmätning. Serie 22 gav lägst uppmätt resistans och var den starkaste ledande kandidaten, men lokala rödkorrosionsfynd i ACT1 kräver fortsatt kontroll av korrosionsrisken. Serie 24 förblev den skyddande referensen men uppträdde elektriskt isolerande, medan serie 27 gav det bästa ACT1-resultatet bland de pulverlackerade systemen utan att uppvisa mätbar ledningsförmåga. Resultaten visar att val av ytbehandling kräver en balans mellan elektrisk funktion, korrosionsskydd och mekanisk och miljömässig hållbarhet.

Nyckelord
ledande ytbehandling, batteriinneslutning, korrosionsbeständighet, elektrisk ledningsförmåga, fordonshållbarhet

Acknowledgements

I would like to thank my TRATON supervisor Raghda Kalifa for her guidance, support, and trust throughout this thesis work. I am also grateful to Patrik Gustafsson, manager of the department, who together with Raghda supported my onboarding at TRATON.

I would like to thank my KTH mentor and examiner Christopher Hulme for academic guidance, and the Surface Treatment section within Materials Technology at TRATON for project support and access to the industrial context of this work. I am especially thankful to Raghda Kalifa and Moa Eklund for their practical help, experimental guidance, and day-to-day support during the project.

I would also like to thank Mats Randelius for guidance on mechanical testing and UV/weathering measurements, Zheng for advice on corrosion evaluation and the technical framing of the project, and Emma for her practical support and explanations during the DSC work.

I would also like to thank my RISE supervisor Johan Tidblad for his guidance, for introducing me to the facilities during an early tour, and for connecting me with Peter Poikajärvi. I am grateful to Peter Poikajärvi for his support and practical help, particularly with the VDA experiments.

I am grateful to my friends, especially Laieh Jwella and Arvind Guruprasad, for their support during my thesis period. Finally, I would like to thank my family, especially my mother, father, and little brother, for their constant encouragement and support.

Ajai Krishna
Stockholm, September 14, 2026

Contents

1 Introduction 1
- 1.1 Problem Background 1
- 1.2 Purpose and Goals 2
- 1.3 Sustainability and Industrial Relevance 2
- 1.4 Research Question 3
- 1.5 Delimitations 3
- 1.6 Author Contribution 3

2 Background 5
- 2.1 Battery Enclosure Coating Requirements 5
- 2.2 Surface Treatment Functions and Layer Structure 6
- 2.3 Conductive Coating Systems 7
- 2.4 Thermal Stability of Powder Coatings 8
- 2.5 Corrosion and Environmental Degradation 8
- 2.6 Zinc-Nickel Coatings and Passivation 9
- 2.7 Adhesion and Mechanical Durability 9
- 2.8 Literature Gap and Thesis Contribution 10
- 2.9 Previous Work and Standards 10

3 Materials and Methods 11
- 3.1 Coating Systems and Substrates 11
- 3.2 Sample Preparation 11
- 3.3 Thickness Measurement 12
- 3.4 Conditioning Routes 13
- 3.5 Adhesion and Mechanical Durability Methods 16
- 3.6 Electrical Conductivity Testing 20
- 3.7 Thermal Analysis and Differential Scanning Calorimetry 22
- 3.8 Corrosion Testing 23
- 3.9 Chemical Resistance Testing 23
- 3.10 UV/Weathering, Colour, and Gloss Measurement 24
- 3.11 Microscopy and SEM/EDS 25
- 3.12 Data Analysis 26

4 Results 27
- 4.1 Coating Thickness and Surface Observations 27
- 4.2 Electrical Conductivity 28
- 4.3 DSC Thermal Analysis 30
- 4.4 Adhesion and Mechanical Durability 32

4.5 Corrosion Testing 41
4.6 Chemical Resistance 42
4.7 UV/Weathering Exposure 43
4.8 Comparative Performance Summary 47

5 Discussion 49
5.1 Interpretation of Coating-System Performance 49
5.2 Methodological Strengths and Limitations 50
5.3 Industrial Relevance 51
5.4 Societal and Ethical Reflection 51
5.5 Use of Generative AI 52

6 Conclusions 53
6.1 Conclusions and Recommendation 53
6.2 Future Work 54

Bibliography 55

A Supplementary Experimental Material 58
A.1 DSC Thermal Analysis Result Graphs 58
A.2 Supporting Optical Cross-Section Images 59
A.3 Detailed Wet-Conditioned Adhesion Images 59

1 Introduction

Electrified heavy vehicles place demanding functional requirements on battery enclosure components. The enclosure lid must be protected against corrosion and mechanical damage, but selected fastening and grounding locations must also provide reliable electrical contact. A thick protective coating can improve corrosion resistance and mechanical durability, but it can also electrically insulate the surface and require local coating removal around grounding points. Such local removal adds manufacturing complexity and interrupts the protective surface treatment at a region that must still withstand corrosion and environmental exposure. The engineering problem in this thesis is therefore to identify whether alternative surface-treatment systems can improve electrical conductivity while retaining sufficient automotive durability.

The thesis work was carried out by the author at TRATON within Materials Technology, Surface Treatment, as part of the master's degree project at KTH. The project also involved support from RISE, particularly for cyclic corrosion exposure. The thesis evaluates conductive surface-treatment and paint systems for battery enclosure lids used in electrified Scania trucks and buses. The systems are compared with the current reference coating system, labelled *Series 24* in the project sample plan, using a set of characterization and durability tests.

1.1 Problem Background

The current reference coating system, *Series 24*, is a comparatively thick powder-coated system used as the protective benchmark because it provides strong corrosion protection. However, its thick powder-paint structure also gives poor electrical conductivity. In practice, electrical contact at bolted grounding points can therefore require local coating removal, for example by laser cleaning around bolt locations to expose a more conductive contact surface. This extra operation adds manufacturing complexity and creates a locally exposed region where the protective coating system has been deliberately interrupted. The same area must then satisfy both electrical-contact and corrosion-protection demands, making it a critical point in the component design.

The industrial motivation is therefore to investigate whether a surface treatment can provide sufficient electrical conductivity without requiring local removal of

the coating below bolts. If the coating itself can support the required electrical contact, the lid and the bolted region can remain covered by the same surface-treatment system, reducing the need for a separate contact-preparation step and avoiding intentional exposure of the underlying material. In addition to conductivity, thermal stability is relevant because an organic coating with too low a glass-transition-related thermal response could soften under elevated temperature, affect bolt clamping stability, and thereby reduce contact reliability. The central trade-off is therefore between thick protective systems, which are expected to provide good corrosion resistance and mechanical durability but weak conductivity, and thinner conductive systems, which are expected to improve electrical performance but may be more vulnerable to coating damage or corrosion degradation.

The battery enclosure lid requirement level is confirmed from drawings as C3 in the Scania surface-treatment requirement framework. In this code structure, the letter describes the finish class and the number describes the exposure level. Thus, A1 can be understood as a higher-finish and milder-exposure case, B2 as an intermediate case, and C3 as a hidden or chassis-type good-finish part with intense exposure. For the battery enclosure lid, this means that the part is not treated as a decorative exterior body panel, but it is still located outside the vehicle environment and must tolerate moisture, salt, road dirt, and temperature cycling.

1.2 Purpose and Goals

The purpose of the thesis is to characterize and compare alternative conductive coating systems for battery enclosure lids against the current Scania reference system. The comparison includes coating thickness, adhesion-related behavior, chemical resistance, UV/weathering response, corrosion performance, mechanical durability, microscopy-supported interpretation, thermal-analysis evidence for powder coatings, and electrical conductivity or resistance measurements.

The practical goal is to support a balanced recommendation for continued evaluation of surface-treatment systems. The academic goal is to interpret the measured behavior as a materials characterization problem, connecting coating structure and thickness to electrical conductivity and durability.

1.3 Sustainability and Industrial Relevance

Surface treatment is also an industrial sustainability question. Coating choices influence not only the service life of the vehicle component, but also the energy use, water use, chemical consumption, waste handling, and process complexity associated with manufacturing. A coating system that gives durable corrosion protection can reduce repair, rework, and premature replacement, while a system that also provides reliable electrical contact can reduce the need for additional local coating-removal operations around grounding points.

For this thesis, sustainability is therefore treated in a practical engineering sense: the preferred coating system should support electrified heavy-vehicle function while avoiding unnecessary loss of durability, extra processing steps, or avoidable material and maintenance burden. The work does not perform a full life-cycle

assessment, but the comparison is intended to support more responsible surface-treatment selection under real industrial constraints.

1.4 Research Question

The primary research question is:

The comparison is based on measured electrical response together with durability indicators from corrosion, adhesion, mechanical, chemical, weathering, microscopy, and thermal characterization.

> Which investigated surface-treatment system provides the most favourable measured compromise between electrical conductivity and durability indicators for battery enclosure lid applications?

The supporting questions are:

- How do the investigated coating systems differ in thickness and initial surface condition?
- How do the systems respond to adhesion, mechanical, chemical, weathering, thermal, and corrosion exposures?
- Does a thinner conductive coating system provide an acceptable durability compromise compared with the current reference coating?
- Can one candidate, particularly the intermediate-thickness powder coating system, be identified as a promising compromise for further qualification?

1.5 Delimitations

The work is limited to the coating systems and production-intent battery enclosure lid material supplied for the project. The panels are cut samples from production parts rather than field-used components. Edge corrosion is outside the intended scope because cut edges were taped before testing. The thesis does not aim to optimize coating formulations, develop a new coating chemistry, or define final production acceptance criteria. The electrical measurement is limited to comparative dry-circuit screening on as-coated coupons; it does not validate the final assembled bolted interface. Proprietary supplier details and acceptance limits that were not available within the project scope are therefore not used to support the coating recommendation.

1.6 Author Contribution

The author's contribution comprised thesis planning, sample preparation, coordination and execution of laboratory measurements, result compilation, comparative interpretation, and thesis writing. TRATON laboratories provided equipment and technical support. RISE performed the VDA 233-102 salt-mist-based accelerated cyclic corrosion exposure and supported preparation and analysis of microscopy specimens using scanning electron microscopy with energy-dispersive X-ray spectroscopy (SEM/EDS). Cotec Labs performed the ACT1 rain-based accelerated cyclic corrosion exposure. The author evaluated and synthesized the resulting evidence into the final surface-treatment comparison.

Figure 1.6.1: Example of local coating removal around an M8 bolt location on a battery enclosure lid. The laser-removed region exposes a more conductive contact surface for the bolted joint, illustrating the practical grounding-related challenge behind the coating-system comparison in this thesis.

2 Background

The coating systems considered in this thesis are not evaluated as decorative finishes alone, but as multifunctional surface systems for an electrified vehicle component. The background chapter therefore focuses on the mechanisms that connect coating architecture to corrosion protection, electrical continuity, adhesion, mechanical durability, and environmental stability. This provides the basis for interpreting why a coating that performs well in one function may fail to meet the complete battery-enclosure requirement.

2.1 Battery Enclosure Coating Requirements

Battery enclosure lids in electrified heavy vehicles require a coating system that protects the underlying metallic component while preserving required electrical functionality. The coating must resist corrosion, remain adherent after environmental exposure, tolerate mechanical damage mechanisms such as impact and chipping, and remain stable under automotive weathering and chemical exposure. For this project, corrosion resistance is currently treated as the highest-priority property, followed by adequate conductivity and then adhesion and mechanical performance.

In the experimental evaluation, these requirements are translated into measurable responses rather than treated as general qualities. Electrical function is assessed through low-resistance dry-circuit measurements over a defined contact spacing, coating thickness is reported in micrometres, adhesion and mechanical durability are rated after standardized cutting, impact, water-jet, cupping, hardness, and scratch exposures, and corrosion performance is judged from visible rusting, white corrosion products, blistering, and scribe-creep behaviour after accelerated cyclic exposure. The coating-selection problem is therefore quantitative in practice, even though the final decision must combine several non-equivalent performance measures.

This type of coating selection is a common difficulty in multifunctional surface engineering. Organic coating literature usually treats barrier protection, adhesion, and coating integrity as central to corrosion resistance because the coating must restrict transport of water, oxygen, ions, and other aggressive species to the substrate [1]. Conductive-coating literature, in contrast, often emphasizes the forma-

tion of electrical pathways through metallic phases, carbon-based fillers, or thin conductive layers [2, 3]. These two design directions can conflict. A coating architecture that improves environmental isolation may also interrupt electrical contact, while a thinner or more conductive surface may provide less tolerance against corrosion, defects, or mechanical damage. The literature review is therefore used here to connect these mechanisms to the practical comparison of the four supplied coating systems.

2.2 Surface Treatment Functions and Layer Structure

Surface treatment is used to provide a combination of appearance, corrosion protection, and functional surface properties. In an automotive coating system, these functions are usually distributed across several layers rather than carried by a single visible surface. A generic painted system can be understood as a topcoat, primer, pretreatment, and substrate. The topcoat contributes appearance, UV stability, chemical resistance, and scratch resistance. The primer supports topcoat adhesion, surface levelling, moisture-barrier behavior, and corrosion protection. The pretreatment supports adhesion between the substrate and the coating system and can also contribute to corrosion resistance.

The experimental programme therefore investigates the coating system at several functional levels. UV/weathering and chemical resistance mainly assess surface and topcoat response, while cross-cut, knife-edge, water-jet, stone-chip, and mechanical tests assess coating integrity, interlayer adhesion, and resistance to damage. Corrosion testing assesses barrier behavior, metallic coating response, pretreatment effectiveness, and degradation around defects. Conductivity testing assesses the electrical behavior of the whole contact stack, including any insulating organic layers or passivating films.

The distinction between organic and inorganic surface treatments is also important. *Series 24* and *Series 27* are powder-paint systems that behave primarily as organic barrier coatings. In contrast, *Series 22* and *Series 23* are thin zinc-nickel/passivation systems with a metallic coating character. These systems can offer better electrical contact, but their corrosion and durability behavior must be interpreted through metallic coating, passivation, and corrosion-product mechanisms rather than through organic barrier behavior alone.

From an electrochemical perspective, an organic barrier coating protects the substrate mainly by slowing the transport of electrolyte, oxygen, and aggressive ions to the metal surface. Its corrosion resistance therefore depends not only on coating thickness, but also on coating continuity, adhesion, defect density, and the ability of the coating stack to resist underfilm transport once a scratch, chip, or edge defect is formed [1]. A passivated zinc-nickel coating works differently. The metallic zinc-nickel layer can provide electrical continuity, while zinc-rich corrosion products and the passivation film can reduce the rate of further electrochemical attack. The passivation layer is therefore important because it modifies the surface reaction kinetics and corrosion-product formation, but it may also influence contact resistance at electrical interfaces [4, 5].

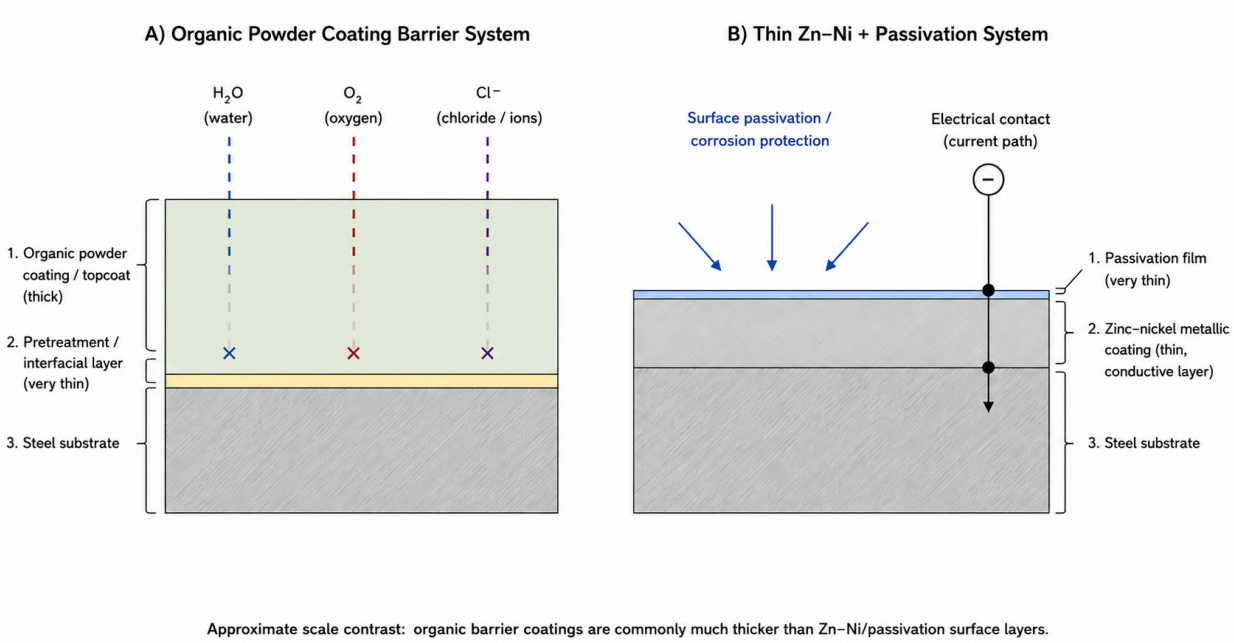

Figure 2.2.1: Conceptual comparison of a thick organic barrier coating architecture and a thinner zinc-nickel/passivation architecture on steel. The schematic illustrates the difference between transport-limiting barrier protection and a metallic/passivated surface layer that can also support electrical contact. The mechanism framing follows the corrosion-protection and zinc-nickel/passivation literature discussed in the text [1, 4, 5]. The schematic was generated with generative-AI assistance and reviewed by the author.

2.3 Conductive Coating Systems

In this thesis, a conductive coating system means a surface treatment intended to provide sufficient grounding or charge-dissipation performance while still functioning as a protective automotive coating. Conductivity is not treated as an isolated maximum-value target. A highly conductive system is not useful if it cannot survive corrosion, chipping, or environmental aging in the battery enclosure application.

The investigated systems include thin zinc-nickel/passivation systems and powder coating systems. The thin metallic character of the zinc-nickel/passivation systems provides a plausible route to lower electrical resistance. The powder coating systems provide thicker organic barriers, and the reference system is known to have poor conductivity because of its comparatively thick insulating structure.

Literature on conductive coatings supports treating electrical performance as a structure- and formulation-dependent property rather than a simple coating label. Conductive paint studies show that resistivity depends strongly on conductive phase content, filler network formation, and measurement method [2]. Broader reviews of conductive coating materials emphasize that conductive fillers, metallic particles, film formation, and deposition route all affect whether an electrically useful pathway is formed [3]. Percolation concepts are most directly relevant for filled organic coatings, where conductivity can increase sharply once a connected conductive network forms [6]. The present thesis does not treat electromagnetic

interference (EMI) shielding as the main topic, but EMI and grounding literature is useful background because both depend on electrical continuity and on reporting resistance or resistivity in a reproducible way [7].

For bolted grounding points, the coating problem is not only whether the surface is conductive in an isolated measurement. The coating also affects whether a stable electrical contact can be maintained after fastening and exposure. If an insulating coating must be removed locally, the exposed region can become a weak point for corrosion protection. If an organic coating softens at elevated temperature, changes in local contact pressure or clamping stability can reduce the reliability of the electrical path. For this reason, the present comparison includes both electrical resistance measurements and thermal analysis data for the powder-painted systems.

2.4 Thermal Stability of Powder Coatings

Powder coatings are organic polymer-based systems, so their mechanical response can change with temperature. The glass-transition-related response is relevant because a coating that softens at elevated temperature may deform more easily under load. In the present application, this matters for bolted contact regions: changes in coating stiffness or deformation around the joint could affect local clamping and therefore contact reliability. Thermal analysis is therefore included for the powder-painted systems as supporting evidence, rather than as a standalone coating-ranking method.

2.5 Corrosion and Environmental Degradation

Corrosion behavior is central to the project because battery enclosure components are exposed to demanding vehicle environments. Two accelerated cyclic corrosion methods were used: VDA 233-102 and ACT1 according to Scania STD4319. Both methods repeatedly vary temperature, humidity, wetting, drying, and salt exposure; they differ in their detailed cycle profiles, program durations, and evaluation routes. Chemical resistance and UV/weathering exposures complemented the cyclic corrosion methods by assessing surface degradation, corrosion spread from scribes or defects, blistering, rust formation, white corrosion products, gloss change, colour change, and other visible failure modes.

SEM/EDS confirmed a steel substrate through the iron-rich substrate signal. Layers rich in zinc and nickel were identified in *Series 22* and *Series 23*. A zinc-rich substrate-side layer was visible in the powder-coated *Series 24* system. These qualitative elemental observations provide the coating-stack basis used in the corrosion interpretation.

The literature review is therefore used mainly to support the durability-versus-conductivity trade-off. Conductive or filled organic coatings can introduce a balance between electrical pathways and barrier performance, where increasing conductive pathways may also affect porosity, interfacial transport, or corrosion protection [8]. General corrosion-protection coating literature also emphasizes barrier protection, adhesion, coating integrity, and service-life extension as central functions of coating systems [1].

2.6 Zinc-Nickel Coatings and Passivation

The thin conductive candidate systems in this thesis include zinc-nickel coatings with passivation. Such coatings are relevant because they can combine metallic electrical continuity with corrosion-protection functions. Their behavior is not identical to either pure zinc coatings or organic barrier coatings. Literature on electrodeposited Zn–Ni coatings shows that corrosion resistance can depend strongly on nickel content. Lambert, Hart, and Townsend reported maximum salt-spray resistance for electrodeposited Zn–Ni coatings around 12 % to 15 % Ni and described corrosion as involving preferential zinc dissolution, development of a nickel-rich residual phase, zinc corrosion products, and a remaining composite layer that contributes barrier protection [4]. This mechanism is useful for interpreting white or grey corrosion products on the thin Zn–Ni/passivation systems without treating them as simple pure-zinc corrosion.

Passivation adds another level of complexity because the passivation film may influence both corrosion resistance and contact resistance. Recent work on black passivation films on Zn–Ni alloy coatings showed that a passivated Zn–Ni system can be designed for both corrosion resistance and low contact resistance, with contact resistance tracked before and after neutral salt spray exposure [5]. That study was performed for aerospace AA2024 connector components rather than steel battery enclosure lids, so its numerical results are not used as direct benchmarks here. Its value for the present thesis is conceptual: passivation chemistry, film structure, corrosion-product formation, and contact-resistance evolution can all affect whether a conductive metallic coating remains electrically useful after corrosive exposure.

2.7 Adhesion and Mechanical Durability

Adhesion and mechanical durability describe the ability of the coating to remain attached and protective under mechanical and environmental loading. Relevant loading routes include cutting, impact, water-jet exposure, scraping, thermal cycling, moisture, and low-temperature conditioning. The experimental program included cross-cut testing, stone-chip resistance testing, high-pressure water-jet adhesion testing, knife-edge adhesion assessment, cupping/extensibility testing, pendulum hardness, and a constrained scratch-visibility assessment.

For protective coatings, adhesion and resistance to mechanical damage are not secondary appearance properties. Loss of adhesion, cracking, chipping, or coating removal can create local pathways for electrolyte transport and expose the substrate. This reduces the effective corrosion protection even if the intact coating has good barrier properties [1]. For this reason, adhesion and mechanical durability tests are used as complementary indicators of whether a coating system can remain protective after local damage or environmental conditioning. These tests do not measure electrical function directly, but they are important for interpreting whether a conductive coating architecture can retain sufficient protective performance in an automotive use case.

2.8 Literature Gap and Thesis Contribution

Taken together, the literature shows that corrosion protection, electrical continuity, thermal stability, and adhesion are often studied as separate coating-performance topics, while industrial coating selection for battery enclosure components requires these functions to be evaluated together. Conductive coatings, Zn–Ni coatings, passivation films, corrosion-protection coatings, and conductive filler networks are established research topics. However, these sources generally address individual material systems, laboratory formulations, or application domains such as conductive paints, aerospace connector coatings, or EMI shielding. They do not directly answer the practical selection question in this thesis: which candidate coating system can provide adequate electrical continuity while retaining corrosion resistance, adhesion, mechanical durability, chemical resistance, weathering resistance, and industrial suitability for a Scania battery enclosure lid?

This thesis therefore fills an application-specific gap rather than a coating-chemistry invention gap. The contribution is a standards-guided comparative characterization of several candidate surface treatment systems under Scania-relevant durability and functionality tests, followed by an integrated interpretation of the conductivity-versus-durability trade-off. The selected literature explains why the trade-off exists and what mechanisms may control it; the experimental program evaluates how the supplied coating systems actually behave in the intended industrial context.

2.9 Previous Work and Standards

The test program is connected to Scania standards where available, including conditioning routes based on Scania standard 4113 and the environmental cycle test according to PV1200. Literature sources are used to support the scientific interpretation of conductive coatings, corrosion-protection mechanisms, and electrical-continuity trade-offs; the internal and international standards define the local test execution and rating frameworks.

3 Materials and Methods

Scania internal standards are cited where they guide the test design or interpretation. Deviations from the cited standards are stated explicitly where they affect how the results should be read.

3.1 Coating Systems and Substrates

Four coating systems were investigated using coded series numbers. The current Scania reference coating system is labelled *Series 24* in the project sample plan. SEM/EDS was used qualitatively to identify substrate and coating-layer chemistry; representative SEM cross-sections and EDS maps are presented in Figures 4.1.1 and 4.1.2. The analysis confirmed a steel substrate through the iron-rich substrate signal. It also confirmed zinc/nickel-rich interfacial layers in *Series 22* and *Series 23* and a zinc-rich substrate-side layer in the powder-coated *Series 24* system.

Table 3.1.1: Investigated coating systems and SEM/EDS-supported layer identification.

Series	Description	Thickness mean ± SD	Notes
22	Zinc-nickel with silver passivation	13.2 µm ± 2.4 µm	Thin conductive candidate
23	Zinc-nickel with black passivation	8.9 µm ± 1.1 µm	Thin conductive candidate
24	Axalta powder coating reference	201.0 µm ± 19.7 µm	ED primer; poor conductivity
27	Glossy powder coating	80.9 µm ± 10.5 µm	ED primer; possible compromise

3.2 Sample Preparation

Samples were obtained from production-intent battery enclosure lids supplied directly from manufacturing. The parts were not field-used components. Main me-

chanical and corrosion-type panels were cut to approximately 100 mm by 150 mm, while UV/weathering panels were cut to approximately 100 mm by 50 mm. After cutting, burrs were manually removed by filing and the edges were covered with black tape. Edge corrosion is therefore not evaluated in this thesis.

For traceability, samples are identified as Y26-XX-YY, where XX is the coating-series label and YY is the individual sample number; for example, Y26-24-19 denotes sample 19 from *Series 24*. The full sample allocation matrix is retained in the project documentation, while the thesis states the relevant sample IDs in the corresponding method and result sections.

Separate panels are used for separate conditioning routes. Adhesion and mechanical integrity were evaluated using impact damage from stone-chip testing, high-pressure water-jet exposure to check coating lifting, lattice-cut adhesion by cross-cut testing, knife-edge lifting at a cut mark, and cupping deformation; these methods are described in the sections below. Most experiments use approximately three panels per coating system, although some tests use fewer samples because of availability constraints. Samples were randomly selected from coded batches to reduce selection bias.

Figure 3.2.1: Representative prepared test panels showing taped cut edges and the Y26-XX-YY sample identification format. The overlaid dimension markers indicate the nominal 100 mm by 150 mm size of the main rectangular test panels.

3.3 Thickness Measurement

Coating thickness was measured using an Elcometer 456 coating-thickness gauge and, for the inorganic zinc-nickel systems, supported by the ISO 3497 values reported in the external corrosion documentation. Five local thickness readings

were recorded on each sample, and the instrument-reported average for each sample was noted. The reported series thickness values in Table 3.1.1 were then calculated as the mean of these sample averages. The standard deviation represents sample-to-sample scatter within each coating series, not the within-sample scatter of the five individual point readings. Dry-film thickness is reported together with relevant test results because thicker coatings can improve barrier protection while also increasing the coating thickness that must be considered in electrical contact or grounding measurements.

3.4 Conditioning Routes

Adhesion-related evaluations were performed after several conditioning routes. Standard conditioning used climate room exposure at 23 °C ± 2 °C and 50 % ± 5 % relative humidity for approximately 24 h. Wet conditioning was performed according to the Scania STD4113 conditioning context using full immersion in deionized water for 96 h at 40 °C, followed by approximately 24 h in the climate room before testing [9]. The samples were held on a rack in a covered water bath with mild circulation or stirring. No intentional aeration was used. SS-EN ISO 2812-2:2018 was reviewed as supporting context for water-immersion terminology and reporting details, but STD4113 is treated as the primary conditioning reference for this thesis [10, 9].

Cryogenic conditioning was also treated as an STD4113-guided route and was performed for 24 h at approximately −20 °C, followed by immediate stone-chip testing before significant warming. The surface-treatment requirement level is interpreted through the STD4111 surface-treatment code structure [11]. In this structure, the letter describes the finish classification and the number describes the exposure level. For example, A1 represents a high-finish, lower-exposure type of requirement, B2 represents an intermediate requirement level, and C3 combines finish class C for good-finish hidden or chassis-type parts with exposure level 3 for intense exposure. The battery enclosure lid requirement level was confirmed from drawings as C3.

For the freezer-conditioned samples in this thesis, only stone-chip testing was performed. This choice was made because stone-chip testing represents the harshest adhesion-related impact damage screen in the present test set; therefore, it was considered sufficient for assessing whether cold conditioning caused a severe loss of coating robustness.

PV1200 environmental cycling exposes samples to repeated hot-humid and cold phases to reveal coating or component weaknesses before later adhesion and mechanical evaluation. One PV1200 cycle lasts 720 min (12 h) and includes heating to 80 °C at 80% relative humidity, holding at 80 °C and 80% relative humidity, cooling to −40 °C, holding at −40 °C with humidity uncontrolled under sub-zero conditions, and reheating to 23 °C with relative humidity regulated back to 30% once the temperature reaches 0 °C [12]. The corresponding cycle profile is shown in Figure 3.4.4. The PV1200 standard defines the cycle profile itself. The number of cycles used in this thesis is reported separately as the local Scania test execution rather than as a generic PV1200 requirement.

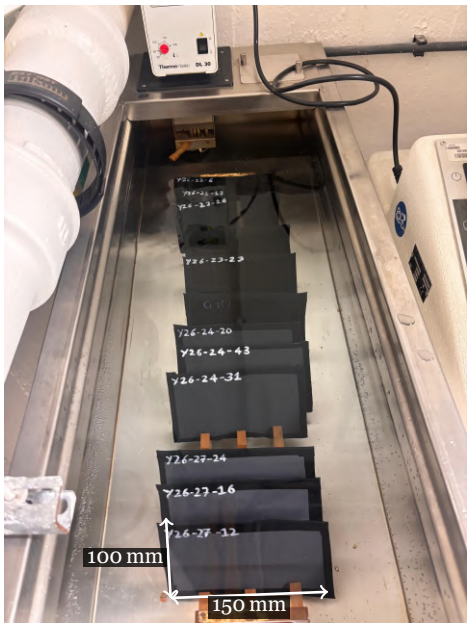

(a) Samples immersed in the water bath.

(b) Covered water bath with controller showing 40.0 °C.

Figure 3.4.2: Wet-conditioning setup used for the STD4113-guided water-bath exposure. The images document that the prepared coated panels were fully immersed in deionized water, held separated on a rack, covered during conditioning, and exposed at 40 °C. The overlaid markers show the panel orientation and approximate test-panel dimensions.

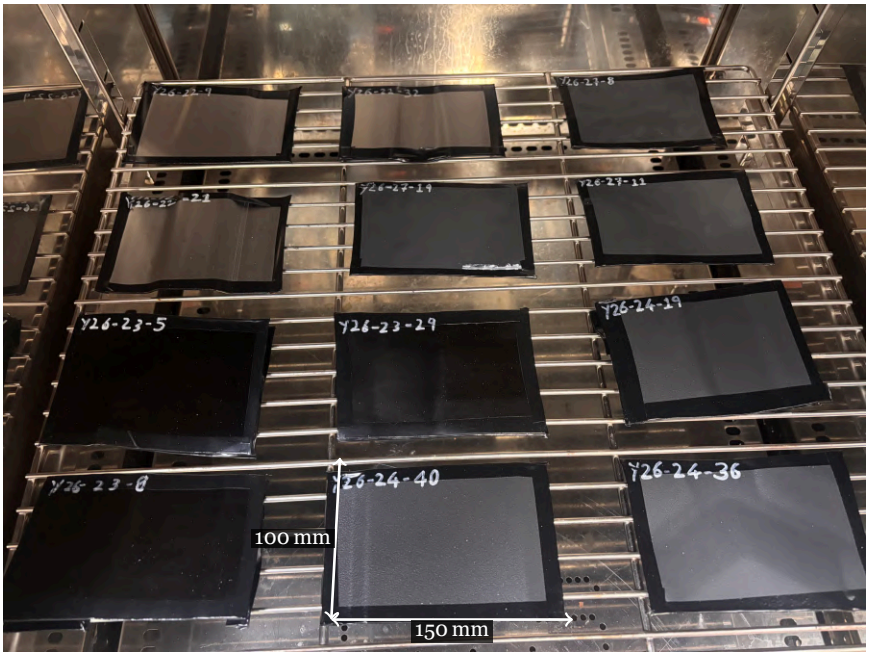

Figure 3.4.3: Coated test panels placed in the CTS chamber for PV1200 environmental-cycle conditioning. The image documents the flat rack placement and separated panel arrangement used before the conditioned adhesion and mechanical evaluations. The overlaid markers show the approximate dimensions of one representative panel.

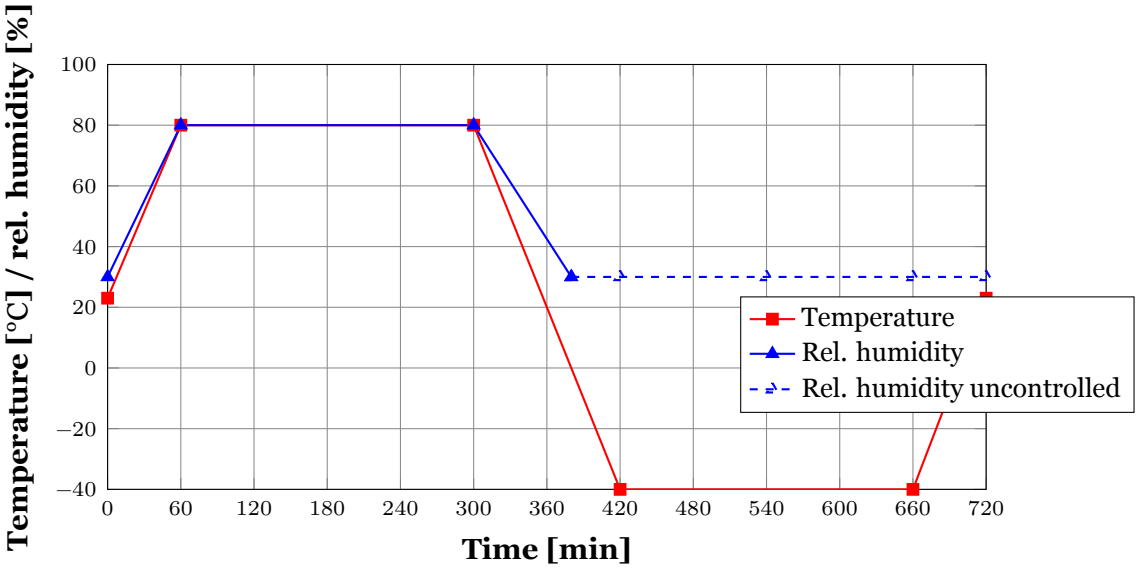

Figure 3.4.4: Temperature and relative-humidity profile for one 720 min environmental cycle according to PV1200, redrawn from the standard [12].

(a) Samples placed in the freezer.

(b) Samples after 24 h freezer exposure.

Figure 3.4.5: Freezer conditioning of prepared coated panels before cold stone-chip testing. The images document the sample placement in the freezer and the exposed sample condition after approximately 24 h at −20 °C.

3.5 Adhesion and Mechanical Durability Methods

Adhesion-related testing includes cross-cut testing, stone-chip resistance testing, high-pressure water-jet adhesion testing, and knife-edge adhesion assessment. The choice and interpretation of these evaluations are guided by STD4113 and the confirmed C3 requirement level interpreted through STD4111 [9, 11]. The following subsections describe the practical role of the individual adhesion-related tests in the thesis.

3.5.1 Stone-Chip Resistance Testing

Stone-chip resistance testing was used to assess the ability of each coating system to resist impact damage from sharp metallic particles. The test is relevant because stone-chip damage can remove coating layers, expose underlying material, and thereby increase the risk of later corrosion. The method was guided by Scania STD4561, which describes gravelometer-style testing of painted surfaces using sharp-edged steel grit and visual grading of the resulting penetration pattern [13]. The standard specifies sharp-edged steel grit according to SS-EN ISO 11124-1, designation ISO 11124 M/HCS/G400, with the grit size defined as 1500 $\pm$ 200 particles per 500 g.

In the standard method, the specimen is mounted in the stone-chip apparatus, exposed to a defined stream of steel grit, brushed lightly after testing, and then evaluated visually. STD4561 specifies approximately 1 kg of steel grit striking the surface within approximately 12 s. In this thesis, a modified execution was used. Each pass used 500 g of steel grit, and each sample was exposed to two passes of approximately 10 s each. This deviation is reported because the total exposure history affects reproducibility and comparison with standard ratings.

The resulting damage was evaluated by comparing the tested surface with the STD4561 reference illustrations. The reference illustration that most closely matches the observed penetration pattern gives the stone-chip grade. In addition to the grade, the affected coating layer was recorded where it could be identified, since shallow topcoat damage and deeper penetration to primer, undercoat, or substrate have different implications for corrosion protection.

3.5.2 High-Pressure Water-Jet Adhesion Testing

Water-jet testing follows the Scania method for determination of adhesion when subjected to high-pressure spraying with water, STD4234 [14]. The main STD4234 parameters used through the equipment “Scania setting” preset are summarized in Table 3.5.2. In this test, a scribed cross is introduced through the coating layers, the scribed region is exposed to a controlled high-pressure water jet, and the resulting damage is evaluated around the scribe.

In the local execution, the equipment display showed the “Scania” module, a testing-period setpoint of 30 s, and a water-temperature setpoint of 55 °C. The sample was positioned so that the scribed cross was centred in the circular holder opening during exposure.

The evaluation records both the type of failure and the extent of damage. Failure type is classified as adhesive failure between layers or between coating and

Table 3.5.2: STD4234 high-pressure water-jet parameters used through the equipment "Scania setting" preset. Pressure and flow depend on the installed nozzle model [14].

Parameter	Setting / requirement	Note
Spray nozzle manufacturer	Spraying Systems Co	Standard nozzle family
Spray nozzle model	1/4MEG 2506-1 or 1/4PMEG 2506-1	Nozzle-dependent pressure and flow
Water pressure	120 ± 3 bar or 68 ± 1 bar	Depends on nozzle model
Water flow	15.0 ± 0.3 kg/min or 11.3 ± 0.3 kg/min	Depends on nozzle model
Test duration	30 s	Per test area
Sweeps in 30 s	30 ± 2	Pendulum sweeping motion
Sweep width	40 ± 1 mm	Defined at test surface
Water temperature	55 ± 5 °C	Heated water jet
Nozzle-to-surface distance	100 ± 3 mm	At 90° to test surface
Scribed-cross orientation	$45° \pm 5°$	Relative to water-jet beam

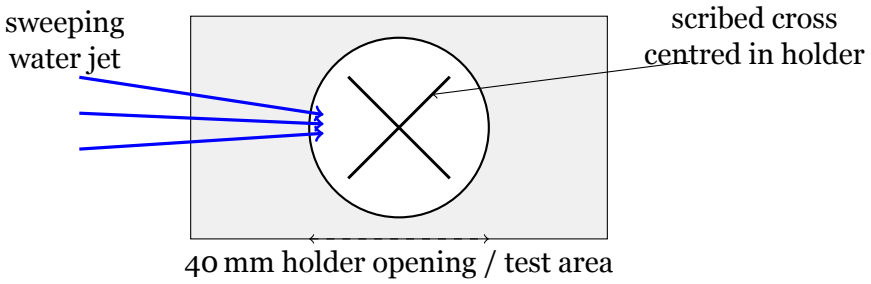

Figure 3.5.6: Schematic representation of the STD4234 high-pressure water-jet adhesion test geometry used for interpretation. The scribed cross is centred in the 40 mm holder opening and oriented approximately 45° to the sweeping water-jet direction.

substrate, cohesive failure within a paint layer, or cohesive failure close to the underlying surface. The extent of damage is rated from 1 to 5 according to the percentage of delaminated test surface, where rating 1 corresponds to 0–5% delamination and rating 5 corresponds to 51–100% delamination. The failure layer or interface was recorded where visible because primer-to-substrate failure and topcoat-layer failure have different implications for protection.

3.5.3 Cross-Cut Testing

Cross-cut testing was performed according to ISO 2409:2020, which evaluates the resistance of a coating to separation after a right-angle lattice pattern has been cut through the coating to the substrate [15]. The rake-like manual tool used in this project is referred to in the standard as a hand-held multi-blade cutting tool. Six parallel cuts are introduced in one direction and a second set of six cuts is introduced perpendicular to the first set, producing a lattice pattern. The test is empirical and should not be interpreted as a direct quantitative adhesion measurement.

The coating condition in the lattice area is visually classified from 0 to 5. Table 3.5.3 summarizes the classification logic used for interpreting the test results. Figure 3.5.7 shows schematic examples of classes 0–4; class 5 is assigned when the flaking is more severe than class 4.

Table 3.5.3: Summary of ISO 2409 cross-cut classification used for thesis interpretation [15].

Class	Affected lattice area	Interpretation used in this thesis
0	0%	Smooth cut edges; no squares detached
1	≤5%	Minor flaking, mainly at cut intersections
2	>5–15%	Flaking along cut edges and/or intersections
3	>15–35%	Larger flaking along edges or within lattice squares
4	>35–65%	Severe flaking; some squares partly or fully detached
5	Worse than class 4	Any degree of flaking that cannot be classified as class 4

3.5.4 Knife-Edge Adhesion Assessment

Knife-edge adhesion assessment was performed according to STD2239, which evaluates coating adhesion by means of a knife edge [16]. In this method, a knife with a well-ground edge is used to scrape through the coating to the substrate. The knife blade is held transverse to the scraping direction and approximately perpendicular to the test surface. After the scratch is made, the coating at the scratch edge is mechanically challenged, and the edge appearance and ease of coating removal are assessed visually.

STD2239 classifies the result from 0 to 3, where lower values indicate better adhesion. Table 3.5.4 summarizes the rating logic in thesis wording.

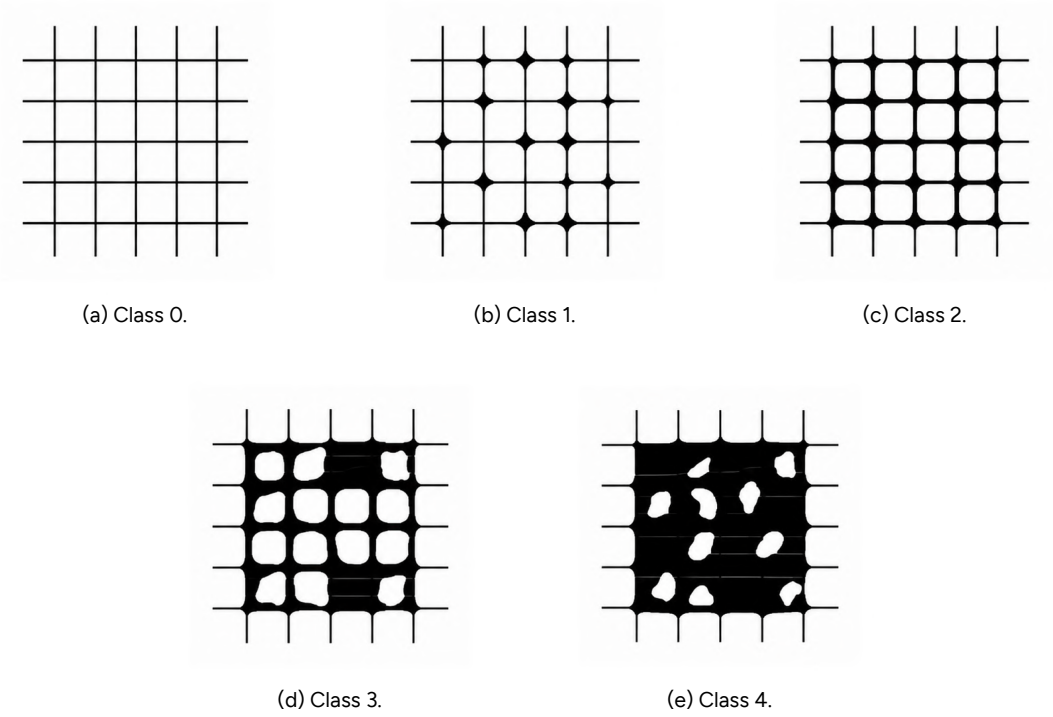

(a) Class 0. (b) Class 1. (c) Class 2.

(d) Class 3. (e) Class 4.

Figure 3.5.7: Visual examples of ISO 2409 cross-cut classifications 0–4, shown as thesis-prepared schematic redraws based on the ISO 2409 classification logic [15]. ISO 2409 classification 5 has no separate visual example in this figure; it is assigned when the flaking is more severe than class 4.

Table 3.5.4: Summary of STD2239 knife-edge adhesion assessment ratings used for thesis interpretation [16].

Rating	Adhesion description	Interpretation used in this thesis
0	Very good	Coating remains attached when mechanically challenged; uniform scratch edge
1	Good	Coating can only be lifted with difficulty; insignificant jaggedness
2	Poor	Coating can be peeled off easily; rough or jagged edge, flakes may chip away
3	Very poor	Coating can be removed in connected patches when mechanically challenged

3.5.5 Cupping, Pendulum Hardness, and Scratch Testing

Mechanical characterization was adapted to the production-intent battery-lid samples available during the test window. The flattest suitable regions of these samples were selected, and the results are used as comparative mechanical evidence for the investigated coating systems.

The cupping/extensibility test was performed using an ERICHSEN Model 202 EM cupping tester and is reported with ISO 1520:2006 as the method reference [17]. One primary sample from each coating series was tested. The coated surface was oriented toward the observation viewpoint, and the indenter displacement in millimetres was recorded at visible damage points. The practical endpoint used for comparison is the larger clearly visible-damage point.

Pendulum hardness was performed according to ISO 1522:2022 using a BYK-Gardner pendulum hardness tester in König mode [18]. The display was set to seconds and the acoustic signal was switched off. The test was applied to the organic/powder coating systems *Series 24* and *Series 27*, where a pendulum damping response is meaningful for the coating film.

Series 22 and *Series 23* were not measured by this method. Their thin inorganic zinc-nickel systems with passivation are not directly comparable to the thicker organic coating films in a pendulum damping test. Measurements were made on selected stable areas where the pendulum could be supported by the two contact balls on the coating surface.

Scratch testing used a BYK-Gardner DUR-O-Test 5810 scratch hardness tester with a 1 mm needle tip. The assessment used replaceable springs with force ranges of 0–3 N, 0–10 N, and 0–20 N. In the laboratory kit these were identified by silver, red, and blue markings, respectively. Each spring was used at stopper scale settings 150 and 300. During each scratch, the needle was pressed until it retracted into the holder and the holder face contacted the sample surface. A line was then drawn across the coating.

The applicable requirement framework specifies scratch-test requirements for A1, A2, B1, B2, C1, and C2 components, but does not define a corresponding requirement for C3 components. The project therefore used the first spring and stopper setting at which the scratch became visible from a normal viewing distance under indoor lighting without close inspection as a comparative visibility threshold between the coating systems.

3.6 Electrical Conductivity Testing

Electrical conductivity was evaluated using a fixed-distance comparative dry-circuit resistance measurement. The purpose of the measurement was to compare the as-coated surface treatments, not to reproduce the final assembled frame, gasket, and bolted contact interface.

Measurements were performed in the environment lab using a Keithley 2010 multimeter. A dry-circuit condition was used, with low voltage and current ($U \leq 20\,\mathrm{mV}$, $I \leq 1\,\mathrm{mA}$) so that possible insulating surface layers would not be broken during the measurement. This low-energy approach is relevant to Scania

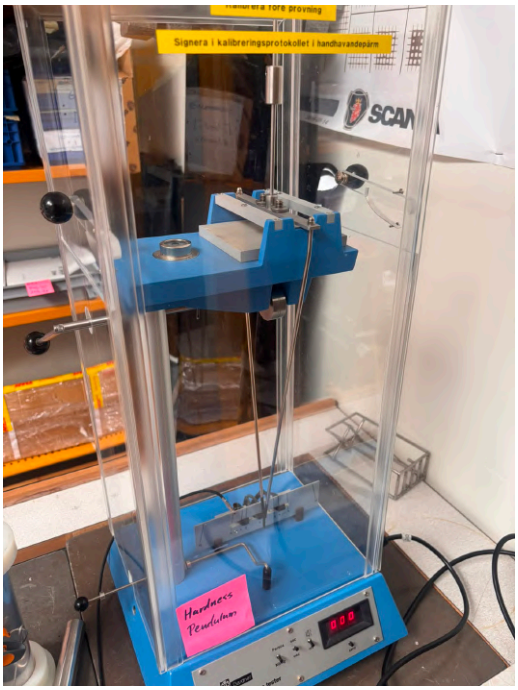

(a) BYK-Gardner pendulum hardness tester.

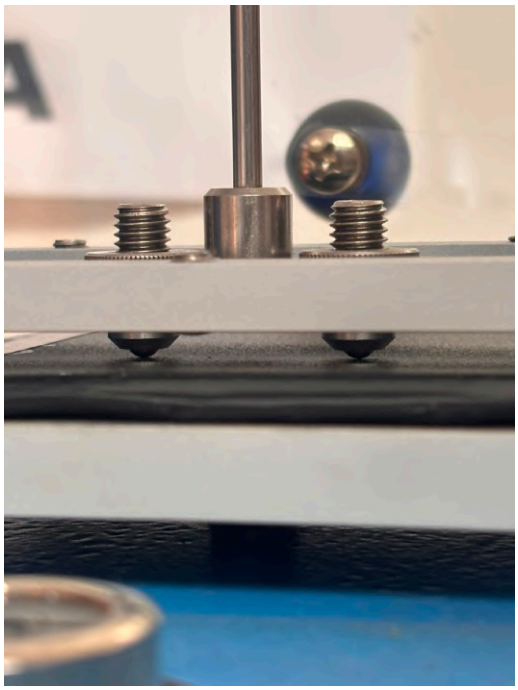

(b) König pendulum contact balls on the coating surface.

Figure 3.5.8: Pendulum hardness setup used for the available-sample ISO 1522-based König damping measurements.

(a) DUR-O-Test 5810 tool marking.

(b) Spring-range label for the scratch tester.

Figure 3.5.9: BYK-Gardner DUR-O-Test scratch hardness tester documentation used for the available-sample scratch assessment.

electrical-conductivity practice because STD4472 includes a dry-circuit measurement route for electrically functional fastener joints, specified at $U \leq 20\,\text{mV}$ and $I \leq 100\,\text{mA}$ [19]. The project-specific coupon screening therefore used the same voltage ceiling and a stricter current ceiling of 1 mA. However, the present thesis did not reproduce the full STD4472 fastener assembly, tightening-torque, bearing-plate, cable-terminal, or voltage-drop correction procedure. Instead, a fixed distance of 50 mm was marked on each coating coupon using a vernier caliper and a white marker. The probes were then placed at the marked points on the as-coated surface. The values fluctuated during measurement; therefore, the lower recurring value that appeared repeatedly was recorded for the conductive samples.

The Keithley instrument was used in a four-wire resistance mode, but the hand-held probe arrangement still produced two effective contact points on the sample surface. The setup therefore compensates lead resistance but does not remove the probe-to-sample contact effect. The method is consequently treated as a comparative surface-response screening method. It is not interpreted as a formal sheet-resistance measurement, a true Kelvin measurement across the coating surface, or assembled-joint contact resistance. No Scania pass/fail acceptance criterion was applied to this coupon screening route, and the values are not compared directly with milliohm-level assembled equipotential-bonding requirements.

3.7 Thermal Analysis and Differential Scanning Calorimetry

Thermal analysis was performed for the powder-painted systems, *Series 24* and *Series 27*, because STD4113 includes a thermal requirement context for organic coatings [9]. The completed laboratory route used differential scanning calorimetry (DSC), and the reported value is the glass-transition temperature, T_g. DSC measures the heat-flow difference between a sample and a reference while both are heated according to a controlled temperature program; the glass transition appears as a step change in the heat-flow signal, and the inflection point of this step was used as the reported T_g value.

Powder-paint topcoat material was scraped from standard-conditioned samples while avoiding ED-primer material as far as possible. The *Series 24* material was taken from sample Y26-24-4. The *Series 27* material was taken from sample Y26-27-21, which had previous physical damage from standard-condition mechanical testing but had not been wet-, cold-, or otherwise specially conditioned. Two replicate cups/pans were prepared for each series. The scraped material was cut into small fragments, placed in aluminium NETZSCH Concavus pans with pierced lids, and sealed using the local crimping device.

The DSC exports identify the instrument as NETZSCH DSC 214 and the program as ISO11357 - PP, from 25 °C to 210 °C at 10 K min^{-1}, using Concavus Al pans with pierced lids and a nitrogen atmosphere. The reported result used for comparison is the DSC glass-transition/inflection value. Actual sample masses were between 5.3 mg and 8.5 mg. Although these masses are below the local manual's general 10 mg to 20 mg guidance, each sample provided appropriate crucible coverage and produced a clearly evaluable transition. The lower masses are therefore reported as method traceability rather than treated as a validity limitation.

3.8 Corrosion Testing

Corrosion testing was performed externally using two accelerated cyclic corrosion methods. The VDA 233-102 exposure was performed by RISE over six weekly cycles; this method combines repeated salt-spray, controlled humidity and temperature, drying, and freezing stages to accelerate corrosion and coating-degradation mechanisms around exposed defects [20]. The evaluation route was split according to coating type.

The inorganic zinc-nickel/passivation systems, *Series 22* and *Series 23*, were evaluated primarily at the three-week checkpoint using an appearance/protection rating framework for metallic coatings. In this framework, the appearance rating R_{A} describes the visible surface appearance after corrosion exposure, especially white-corrosion products, while the protection rating R_{p} describes the degree of protection against base-metal corrosion [21, 22].

The powder-painted systems, *Series 24* and *Series 27*, were evaluated after six weeks using a painted-system scribe-creep method, where corrosion propagation is measured from an artificial scribe in the coating. Maximum propagation was measured from the closest scribe edge after excluding the outer 10 mm at each end of the scribe [23]. This separation avoided applying painted-system scribe-propagation logic to the inorganic surface treatments.

ACT1 accelerated cyclic corrosion testing was performed by Cotec Labs according to Scania STD4319 [24]. A weekly ACT1 cycle alternates controlled humid and dry climates with repeated application of acidified 1 % sodium-chloride solution. The cycle includes high-humidity exposure at 35 °C, drying at 45 °C, and controlled humidity ramps between these conditions. The program length depended on the coating family: *Series 22* and *Series 23* underwent four-week C3-IF zinc-nickel/inorganic-coating programs, while *Series 24* and *Series 27* underwent six-week C3-PP powder-painted programs. The ACT1 results were evaluated using the rating and requirement logic stated in the respective Cotec Labs verification reports rather than imposing a single duration or metric across all four series.

3.9 Chemical Resistance Testing

Chemical resistance testing used a project-specific sponge spotting method guided by the chemical-resistance framework in STD4113 rather than a direct implementation of a single standard exposure method [9]. One sample from each coating series was used: Y26-22-12, Y26-23-25, Y26-24-23, and Y26-27-18. A common alkaline cleaning-agent or laboratory-detergent wash was applied before the chemical spots. Euro 6 B7 diesel was applied for 20 min under small glass covers in a fume hood at room temperature. Isopropanol and Scania coolant diluted 50:50 with water were applied using covered sponges for 24 h. After exposure, excess liquid was absorbed gently using dry tissue, and the dried spots were later wiped gently with water-wetted tissue to reveal possible blistering, delamination, discoloration, or other visible changes. The results are interpreted using ISO 4628-1 as a visual framework for defect quantity/size and intensity of uniform appearance change, while noting that the exposure route itself is a project-specific adaptation [25].

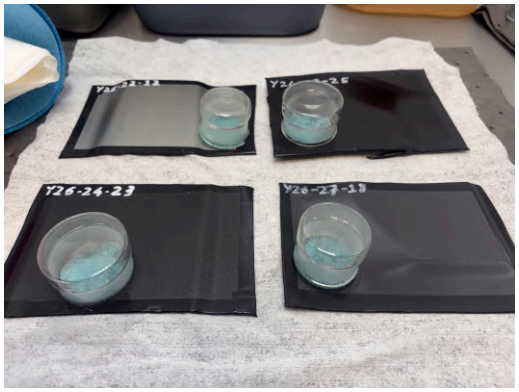

(a) Diesel exposure under small glass covers.

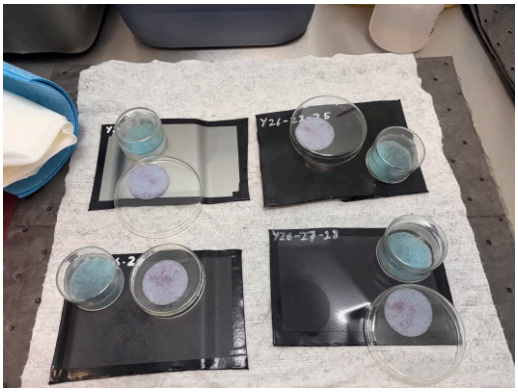

(b) Covered sponge spotting for isopropanol and coolant.

Figure 3.9.10: Chemical-resistance sponge-spotting setup used for the project-specific STD4113-guided exposure route. The images show the prepared coated panels during diesel exposure under small glass covers and during covered sponge spotting for isopropanol and coolant.

3.10 UV/Weathering, Colour, and Gloss Measurement

UV/weathering exposure was performed in a Q-SUN Xe-3-HDS Artificial Weatherproof Aging Test Chamber. The UV/weathering set contained three 50 mm by 100 mm samples from each coating series, giving 12 samples in total. Measurements were made before exposure, after approximately 400 h, and after final removal. The final exposure time was approximately 853 h, based on the chamber-hour counter, and therefore exceeded the 800 h target.

The UV/weathering chamber program is based on SS-EN ISO 4892-2:2013 Method A, Cycle 1, which uses daylight-filtered xenon-arc exposure for artificial weathering [26]. The local setup was confirmed to use broadband total-UV irradiance control. The main exposure-cycle settings used for thesis reporting are summarized in Table 3.10.5. The dry-cycle relative humidity was set locally to 65% RH rather than the 50% RH value listed for the standard cycle; this is reported as a local deviation and is consistent with the higher relative-humidity option noted in the standard for humidity-sensitive materials.

Measurements for UV/weathering included colour and gloss before exposure, at the 400 h checkpoint, and after final removal. Colour was measured using a Konica Minolta CM-700d spectrophotometer as three CIELAB readings per sample, taken at left, centre, and right positions. Gloss was measured using a Rhopoint Glossmeter at 20°, 60°, and 85° according to the ISO 2813 geometry framework [27]. Because the UV samples were visually close to flat but not perfectly flat, seating of the glossmeter was a practical limitation. Baseline gloss was therefore recorded on the flattest or most measurable UV sample from each series, together with one flatter non-UV reference sample per series. Final gloss was measured for all 12 UV samples, but formal baseline-to-final gloss comparison is made only for the four UV samples with matching baseline values. The full final gloss set is retained as supporting trend context.

STD4113 provides the Scania-side context for artificial weathering, gloss, and colour permanence assessment [9]. In this framework, gloss permanence after artificial UV is assessed before polishing using ISO 2813, while colour perma-

Table 3.10.5: UV/weathering exposure-cycle settings used for the Q-SUN xenon-arc chamber program, based on SS-EN ISO 4892-2:2013 Method A, Cycle 1, with the local dry-cycle relative-humidity setting reported separately.

Parameter	Thesis-use setting
Standard basis	SS-EN ISO 4892-2:2013, Method A, Cycle 1
Light-filter route	Daylight-filter xenon-arc exposure
Irradiance control	Broadband total UV, 300 nm to 400 nm
Broadband irradiance	$60\ \mathrm{W\,m^{-2}} \pm 2\ \mathrm{W\,m^{-2}}$
Cycle structure	102 min dry exposure followed by 18 min water spray
Black-standard temperature	$65\ ^\circ\mathrm{C} \pm 3\ ^\circ\mathrm{C}$ during the dry exposure
Chamber air temperature	$38\ ^\circ\mathrm{C} \pm 3\ ^\circ\mathrm{C}$ during the dry exposure
Relative humidity	65% RH dry-cycle setpoint, used instead of the standard-cycle 50 % RH reference value

nence is visually assessed after polishing using ISO 3668 [27, 28]. The final measurements reported here were taken after cleaning and drying, but before any polishing step. They therefore represent the cleaned, unpolished final condition used for the thesis comparison.

3.11 Microscopy and SEM/EDS

Cross-section microscopy was used to examine coating build, visible layer structure, and layer-identity evidence for the four coating systems. Four standard-conditioned samples were selected to represent the unexposed coating systems: Y26-22-22, Y26-23-24, Y26-24-37, and Y26-27-28. Small regions of approximately 15 mm by 10 mm were marked on representative coated areas, cut to approximately 10 mm by 15 mm, mounted, and examined in cross-section. The optical microscopy image metadata list a Zeiss Axio Imager.M2 microscope, Axiocam 305 camera, and Epiplan-Neofluar 20x/0.50 HD DIC objective.

Optical microscopy was treated as supporting evidence. It was used to inspect cross-section quality and compare visible layer structure between coating systems, while coating thickness was reported from the Elcometer dry-film-thickness measurements. Local damage from cutting and mounting was visible in some cross-sections, especially for *Series 24*, so distance annotations in the optical micrographs are treated as local observations rather than final coating-thickness values.

SEM/EDS was used as the primary microscopy method because it provided clearer coating cross-sections and qualitative elemental information. The SEM/EDS specimens were prepared using a conductive hot-mounting route: small pieces were cut from the samples, mounted in black conductive mounting material, ground through progressively finer abrasive papers, and polished in three diamond-paste steps of 3 µm, 1 µm, and 0.1 µm. MD Dac, MD Dur, and MD Chem polishing cloths were used for these polishing steps, respectively. SEM morphology images were

acquired mainly at 5 kV EHT and magnifications of approximately 50x, 150x, and 500x. EDS mapping images were acquired at 20 kV, generally around 250x, with an additional lower-magnification EDS map for *Series 27*. In this thesis, EHT is treated as the accelerating-voltage or beam-energy setting.

The EDS maps are used qualitatively to identify elemental locations in the coating cross-sections. Numerical compositions are not reported because the available EDS outputs are image-based and did not include exported quantitative composition tables.

3.12 Data Analysis

Data analysis is structured around the central requirement of this thesis: the selected surface-treatment system must provide sufficient electrical conductivity without sacrificing the corrosion protection and durability expected for the battery enclosure lid. Each system is therefore evaluated as a multifunctional surface treatment rather than by a single best-performing test result.

The comparison first treats each test route separately, using the applicable rating scale, measured value, or qualitative observation for that method. Corrosion, adhesion, mechanical durability, chemical resistance, UV/weathering response, coating thickness, microscopy evidence, thermal analysis, and conductivity are then brought together in a final comparison matrix. This matrix is used to identify tradeoffs such as high barrier protection with poor conductivity, improved conductivity with weaker environmental durability, or balanced performance across the main requirement areas.

Where replicate measurements are available, results are summarized using simple descriptive statistics such as mean values and observed ranges. Where the dataset is based on limited samples, external laboratory ratings, or visual classifications, the analysis is reported as comparative and evidence-based rather than as a formal statistical ranking.

4 Results

4.1 Coating Thickness and Surface Observations

Thickness measurements show a clear separation between the investigated coating families. *Series 22* and *Series 23* are both thin zinc-nickel/passivation systems, but the available ISO 3497 measurements distinguish them: *Series 22* is thicker, with a measured mean of approximately 13.2 µm, while *Series 23* has a measured mean of approximately 8.9 µm. *Series 27* is an intermediate-thickness glossy powder coating system with a measured mean of approximately 80.9 µm. *Series 24*, the Axalta reference powder coating system, is much thicker at approximately 201.0 µm.

The initial appearance also differs between systems. *Series 22* has a metallic silver appearance, *Series 23* has a black metallic appearance, *Series 24* has a matte textured powder-like surface, and *Series 27* has a glossy surface. These initial visual differences support later interpretation because the systems differ not only in thickness, but also in coating type and surface character.

4.1.1 SEM/EDS Cross-Section Analysis

SEM/EDS is used as the primary cross-section evidence because it combines coating morphology with elemental confirmation.

The SEM images show the coating morphology and interface geometry, while the EDS maps provide chemical confirmation. SEM/EDS confirms a steel substrate, with the substrate signal dominated by iron and with carbon and magnesium also observed locally. The coating-stack hierarchy is consistent with the thickness measurements: *Series 22* and *Series 23* show thin zinc/nickel-rich coating or interfacial bands over the steel substrate, *Series 24* shows a much thicker coating architecture with a visible zinc-rich substrate-side layer, and *Series 27* shows an intermediate coating architecture with a visibly non-uniform interface and local calcium-rich features in the coating region.

The EDS overlays in Figure 4.1.2 are used to confirm the elemental basis of the layer interpretation. The SEM micrographs provide the clearer morphology, while the EDS maps establish the zinc/nickel-rich character of the inorganic sys-

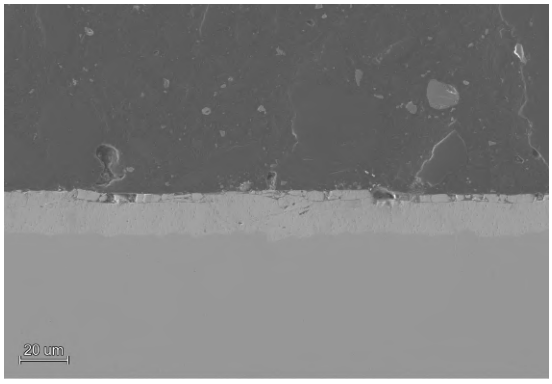

(a) Series 22: thin coating/interface region over steel substrate.

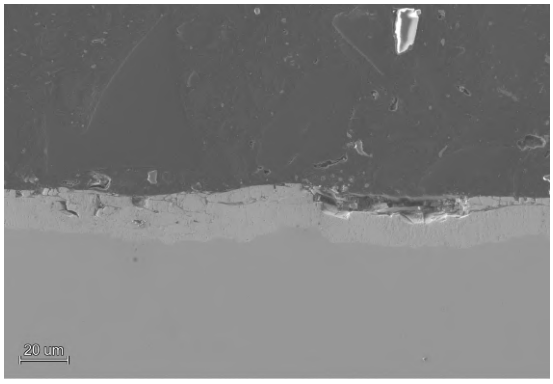

(b) Series 23: thin coating/interface region, similar to Series 22.

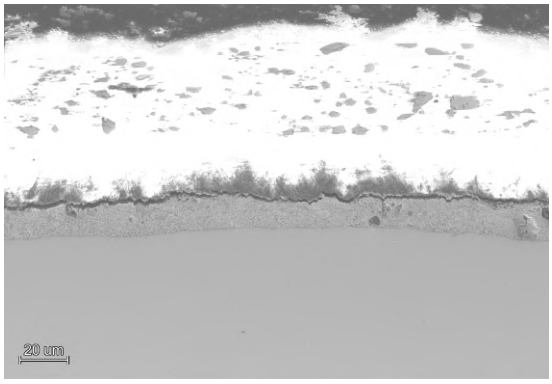

(c) Series 24: thick reference coating architecture.

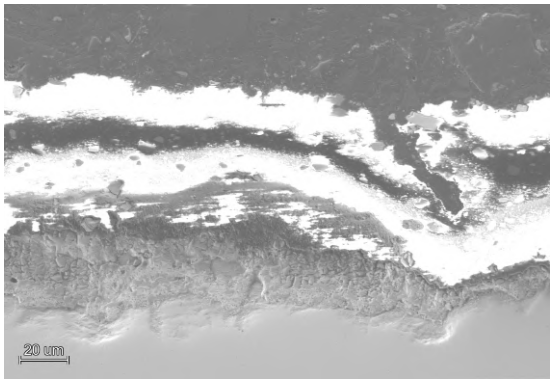

(d) Series 27: intermediate coating architecture with uneven interface.

Figure 4.1.1: SEM cross-section images for the investigated coating systems. Each image includes a 20 µm scale bar. The images show the morphology and layer geometry: thin coating/interface regions for Series 22 and Series 23, a thick coating architecture for Series 24, and an intermediate but visibly uneven coating/substrate-side interface for Series 27.

tems and show a zinc-rich substrate-side layer in the powder-coated *Series 24* system.

Overall, SEM/EDS confirms the distinction between the thin zinc/nickel-rich *Series 22*/*Series 23* systems and the thicker powder-coated *Series 24*/*Series 27* architectures. The elemental maps are interpreted qualitatively and support the coating-system comparison without being used as quantitative composition measurements.

4.2 Electrical Conductivity

The dry-circuit conductivity measurement separated the thin inorganic systems from the powder-painted systems. The screening was performed under low-voltage and low-current conditions of $U \leq 20\,\mathrm{mV}$ and $I \leq 1\,\mathrm{mA}$, using the dry-circuit principle referenced in Scania STD4472 [19]. *Series 22* and *Series 23* gave measurable resistance values over the fixed 50 mm spacing, while *Series 24* and *Series 27* did not give a stable measurable value under the same conditions. The repeat measurement reduced the apparent margin between the two conductive passivation systems compared with the first run, but the ranking remained unchanged. The results are summarized in Table 4.2.1.

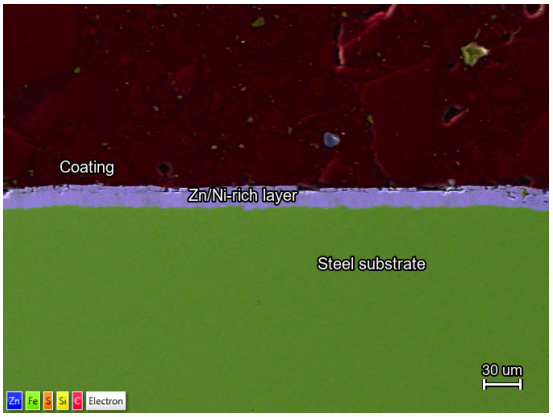

(a) Series 22: zinc/nickel-rich layer over steel substrate.

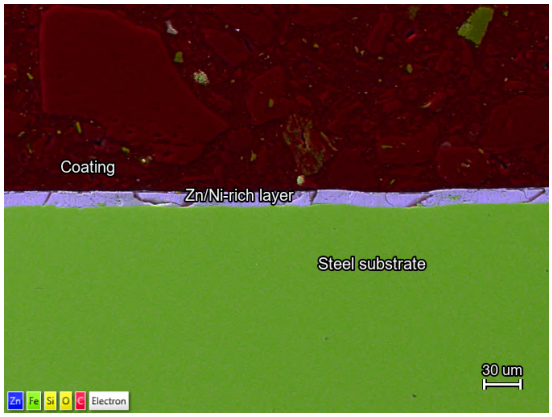

(b) Series 23: thin zinc/nickel-rich layer.

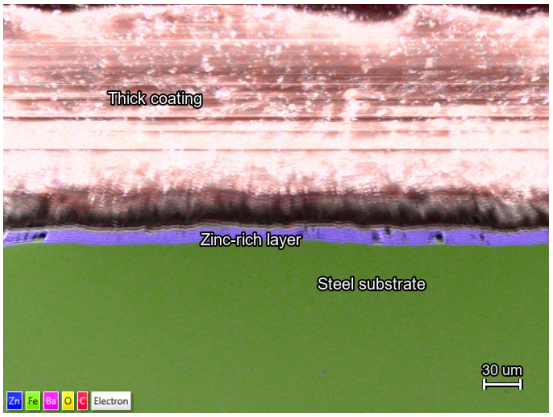

(c) Series 24: thick coating with zinc-rich substrate-side layer.

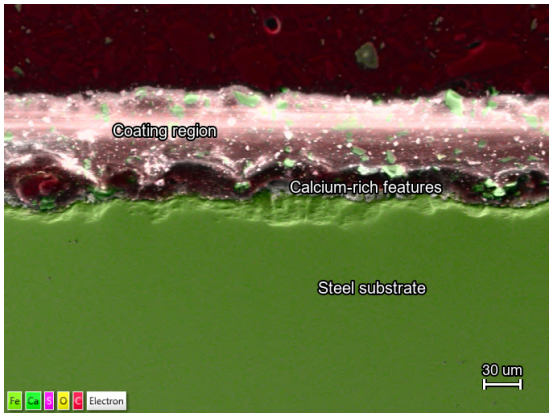

(d) Series 27: coating region with calcium-rich features.

Figure 4.1.2: SEM/EDS overlay maps used for qualitative elemental confirmation. The added labels identify the main regions used for interpretation, and each panel includes a scale bar. The maps confirm a steel substrate and zinc/nickel-rich layers in Series 22 and Series 23. A zinc-rich substrate-side layer is visible in the powder-coated Series 24 system, while the Series 27 map highlights calcium-rich coating features.

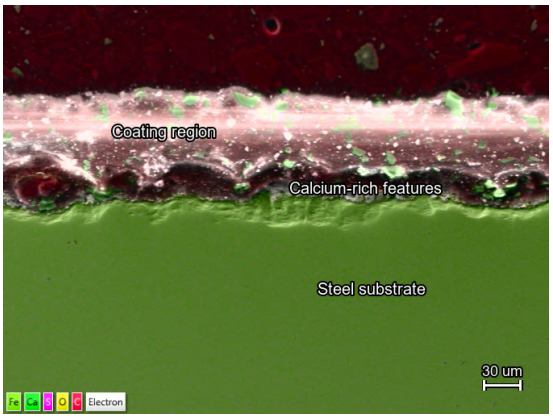

(a) Series 27 EDS location showing calcium-rich coating features.

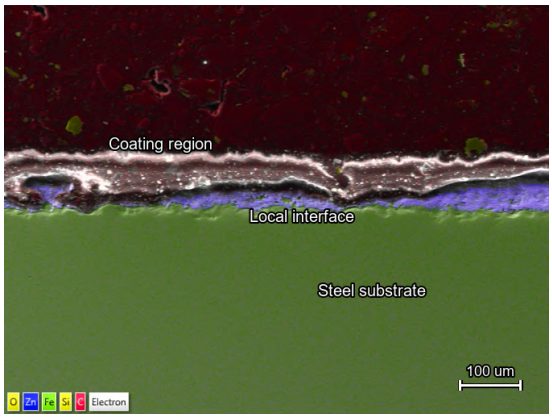

(b) Second Series 27 EDS location showing a separate local cross-section position.

Figure 4.1.3: Two SEM/EDS map locations for Series 27. The added labels identify the main regions used for interpretation, and each panel includes a scale bar. The first highlights calcium-rich features in the coating region, while the second provides a separate local cross-section position. The maps are treated as qualitative evidence of local coating variation.

Table 4.2.1: Comparative dry-circuit electrical-response screening results measured at $U \leq 20\,\mathrm{mV}$ and $I \leq 1\,\mathrm{mA}$ over an approximately fixed 50 mm spacing on the as-coated surface. The results are contact-dependent comparative resistance values and are not interpreted as assembled-joint contact resistance.

Series	Sample	Recorded result	Interpretation note
22	Y26-22-27	approx. 0.11 Ω	Lowest measured resistance; most conductive response in this comparison.
23	Y26-23-9	approx. 0.20 Ω	Conductive, but more contact-sensitive and higher-resistance than *Series 22*.
24	Y26-24-26	No stable measurable value	Insulating behaviour under the applied dry-circuit conditions.
27	Y26-27-9	No stable measurable value	Insulating behaviour under the applied dry-circuit conditions.

The absence of a measurable value for *Series 24* and *Series 27* is not interpreted as literal infinite material resistance. It indicates that no stable resistance value was obtained under the applied $U \leq 20\,\mathrm{mV}$, $I \leq 1\,\mathrm{mA}$ dry-circuit setup. The result supports the coating-family split: *Series 22* and *Series 23* provide the more favourable electrical response, while the powder-coated systems behave as insulating surface treatments under this measurement route. Because the handheld four-wire setup still includes probe-to-sample contact resistance, the values in Table 4.2.1 are used only for comparative screening. They do not validate the milliohm-level resistance expected from a final cover-to-frame bolted equipotential-bonding measurement.

4.3 DSC Thermal Analysis

DSC thermal analysis was performed for the two powder-coated systems, *Series 24* and *Series 27*. The inorganic zinc-nickel/passivation systems, *Series 22* and *Series 23*, were not evaluated by DSC because glass-transition temperature is relevant to polymeric or organic coating constituents rather than to thin inorganic metallic/passivation layers. For the powder-coated systems, the measured T_g values provide an indication of the thermal response of the coating material. The extracted values are summarized in Table 4.3.2.

A representative DSC result graph is shown in Figure 4.3.4. The marked transition region illustrates how the glass-transition temperature was extracted from the heat-flow step, while the complete set of DSC result graphs is included in Appendix A.1.

The duplicate values are internally consistent within each series. *Series 24* has a mean T_g value of 70.7 °C, with a range of 1.1 °C. *Series 27* has a mean T_g value of

Table 4.3.2: DSC glass-transition-temperature results for powder-paint topcoat scrapings from Series 24 and Series 27.

Series	Source sample	Run	Mass	T_g value
24	Y26-24-4	Test 1	7.1 mg	70.1 °C
24	Y26-24-4	Test 2	8.5 mg	71.2 °C
27	Y26-27-21	Test 1	5.3 mg	77.5 °C
27	Y26-27-21	Test 2	5.4 mg	76.5 °C

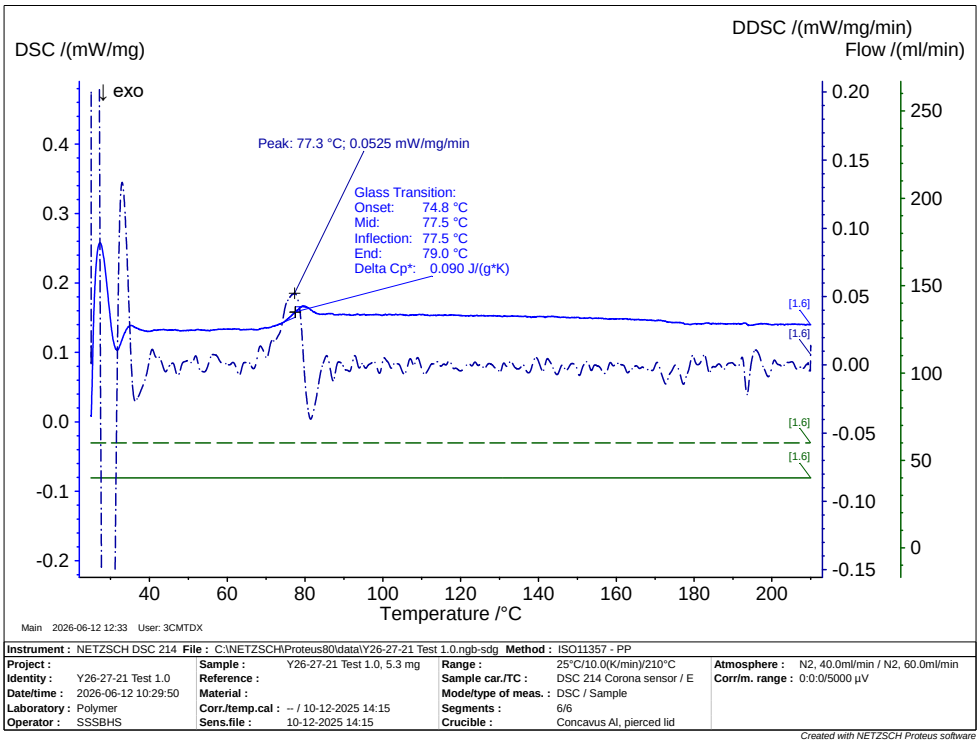

Figure 4.3.4: Representative DSC result graph for Series 27. The graph shows the heat-flow step used to identify the glass-transition temperature, T_g, reported in Table 4.3.2.

77.0 °C, with a range of 1.0 °C. *Series 27* is therefore approximately 6.3 °C higher than *Series 24* in this DSC comparison.

A higher T_g indicates that the coating material remains below its glass-transition region to a higher temperature. *Series 27* can therefore withstand a higher temperature before entering the glass-transition-related softening region than *Series 24*, giving it better resistance to thermally induced softening in this specific cured-coating comparison. This can be relevant for dimensional stability, mechanical response, and contact-area behaviour under elevated service temperatures. The DSC result is nevertheless treated as a supporting thermal-property indicator: it does not by itself establish better overall durability, electrical performance, or assembled-joint stability.

4.4 Adhesion and Mechanical Durability

Adhesion and mechanical durability were assessed using stone-chip, high-pressure water-jet, cross-cut, knife-edge adhesion, freezer-conditioned stone-chip, and constrained cupping tests. The results show strong stone-chip performance for *Series 24*, while the PV1200-conditioned knife-edge assessment reveals greater local top-layer lifting for *Series 24* than for the other systems.

4.4.1 Stone-Chip Grading Basis

Stone-chip grades were assigned by visual comparison with the STD4561 reference illustrations. The reference illustration that most closely matched the observed penetration pattern was used as the Scania grade, as shown in Table 4.4.3. The same grading basis was applied to the standard, PV1200, wet, and freezer conditioning routes.

Table 4.4.3: Grade allocation used for STD4561 stone-chip evaluation. The Scania grade is assigned from the reference illustration that most closely matches the observed penetration pattern [13].

Closest STD4561 reference illustration	Assigned Scania grade
1	1
2	2
3	3
4	4
5	5
6	6

4.4.2 Stone-Chip Results Across Conditioning Routes

Stone-chip testing was performed after standard, PV1200, wet, and freezer conditioning. Table 4.4.4 presents the four routes together so that the conditioning effect can be compared directly. The table reports the assigned grades only; interpretation of the grade changes is given in the following text.

Table 4.4.4: STD4561 stone-chip grades across the relevant conditioning routes.

Conditioning route	*Series 22*	*Series 23*	*Series 24*	*Series 27*
Standard	2	2	1	2
PV1200, 20 cycles	2	2	1	2
Wet, 96 h at 40 °C	2	2	1	2
Freezer, 24 h at approx. −20 °C	2	2	2	2

Across the standard, PV1200, and wet routes, *Series 24* was assigned grade 1 while *Series 22*, *Series 23*, and *Series 27* were assigned grade 2. The freezer route removed this lead: *Series 24* shifted to grade 2, indicating greater top-layer sensitivity during low-temperature impact. For *Series 22* and *Series 23*, small penetration spots may expose the substrate directly because these systems do not contain

an ED primer. For *Series 27*, many light exposed regions are interpreted as ED-primer exposure rather than direct substrate exposure.

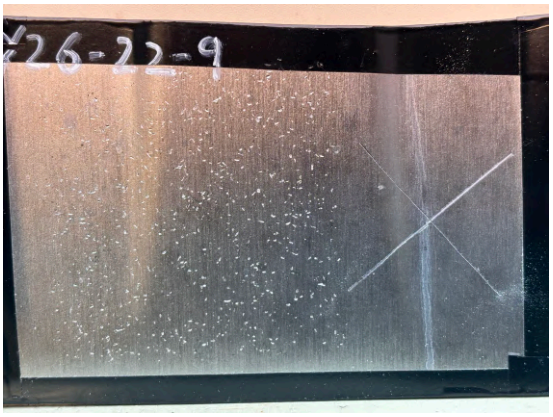

(a) Series 22, Y26-22-9.

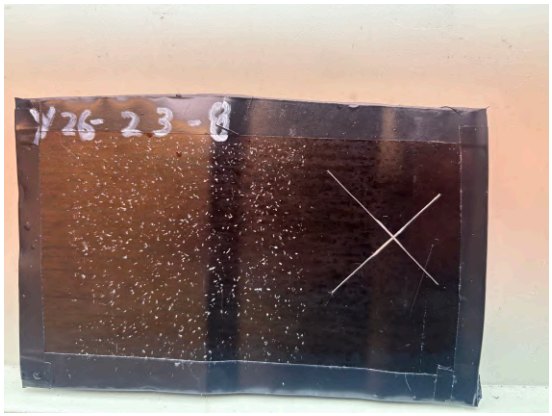

(b) Series 23, Y26-23-8.

(c) Series 24, Y26-24-36.

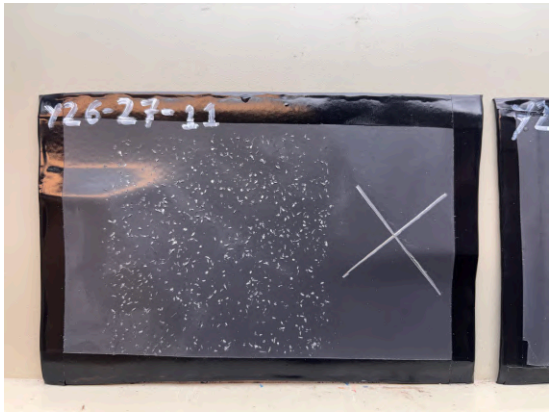

(d) Series 27, Y26-27-11.

Figure 4.4.5: Representative PV1200-conditioned samples after stone-chip and water-jet testing. The stone-chip region is on the left side of each panel and the water-jet region is on the right side. The prepared panels are nominally 150 mm by 100 mm; the visible tested area differs between panels because of masking tape, cropping, and camera perspective.

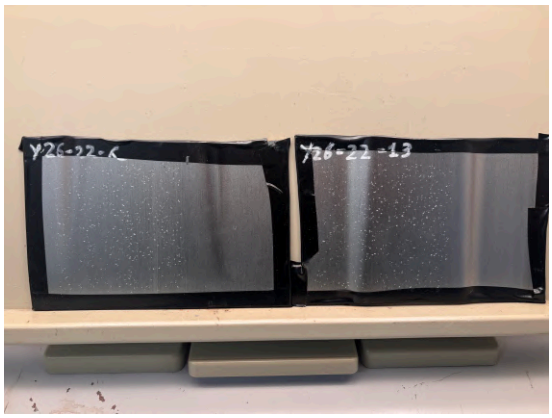

(a) Series 22, Y26-22-6 and Y26-22-13.

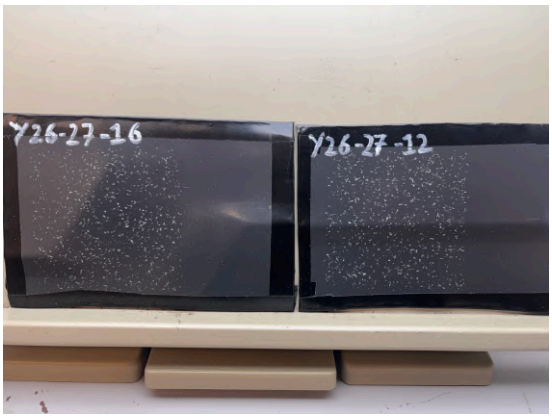

(b) Series 23, Y26-23-28 and Y26-23-23.

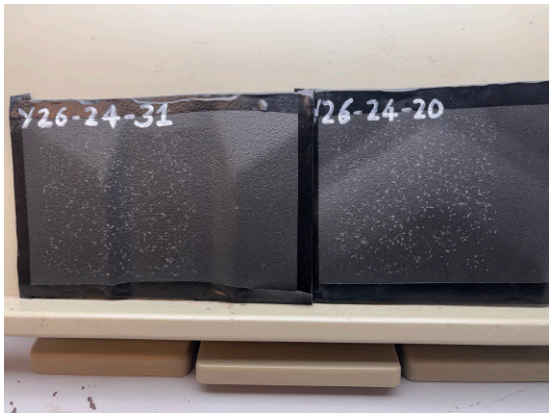

(c) Series 24, Y26-24-31 and Y26-24-20.

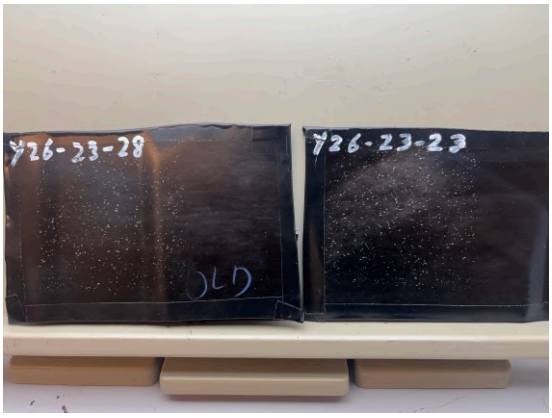

(d) Series 27, Y26-27-16 and Y26-27-12.

Figure 4.4.6: Wet-conditioned samples after stone-chip testing. Series 24 is assigned grade 1, while Series 22, Series 23, and Series 27 are assigned grade 2 based on visual comparison with STD4561 reference illustrations. The images show nominal 150 mm by 100 mm prepared panels, with the visible area affected by masking and image cropping.

(a) Series 22, Y26-22-28.

(b) Series 23, Y26-23-9.

(c) Series 24, Y26-24-42.

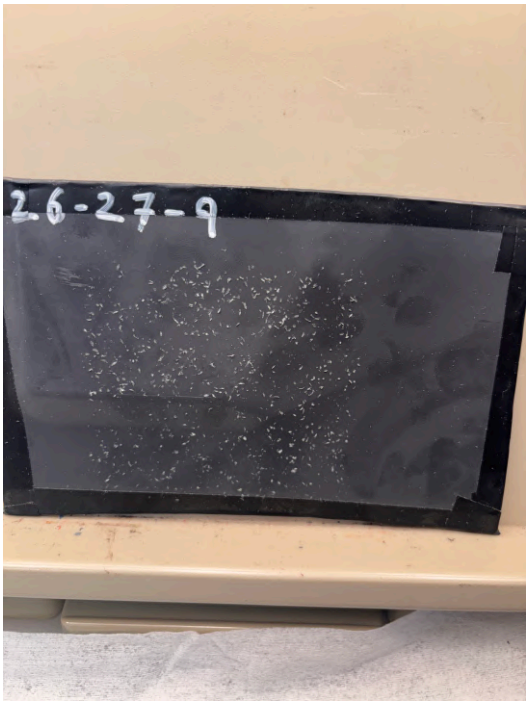

(d) Series 27, Y26-27-9.

Figure 4.4.7: Freezer-conditioned samples after immediate stone-chip testing. Series 24 shows a stronger change relative to its PV1200-conditioned result, shifting from grade 1 to grade 2, while the other series remain broadly similar to their PV1200-conditioned outcomes. The samples follow the same nominal $150\ \mathrm{mm}$ by $100\ \mathrm{mm}$ prepared-panel format; apparent panel size differs between photographs because of rotation, masking, and camera perspective.

4.4.3 Water-Jet Results Across Conditioning Routes

High-pressure water-jet testing was performed after standard, PV1200, and wet conditioning. All evaluated systems received STD4234 rating 1 in every route, corresponding to none or negligible delamination from the scribed test area. Table 4.4.5 summarizes the water-jet results across the three conditioning routes.

Table 4.4.5: STD4234 water-jet ratings across the relevant conditioning routes.

Conditioning route	*Series 22*	*Series 23*	*Series 24*	*Series 27*	Main observation
Standard	1	1	1	1	None to negligible delamination.
PV1200, 20 cycles	1	1	1	1	No broad adhesion failure; *Series 23* showed slight discoloration.
Wet, 96 h at 40 °C	1	1	1	1	None to negligible delamination; *Series 23* showed discoloration.

The unchanged rating across the three conditioning routes indicates that no broad water-jet adhesion failure was detected. The *Series 23* discoloration is retained as a surface-appearance observation rather than an adhesion failure because STD4234 evaluates delamination.

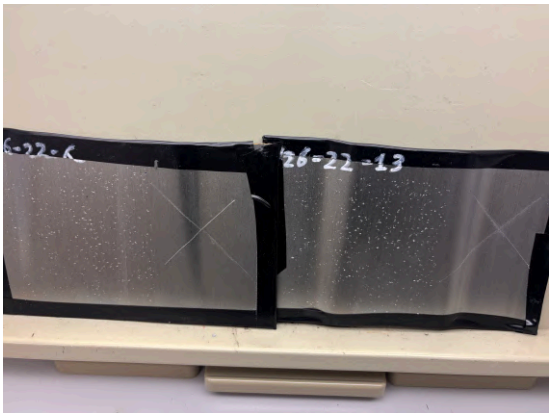

(a) Series 22, Y26-22-6 and Y26-22-13.

(b) Series 23, Y26-23-23 and Y26-23-28.

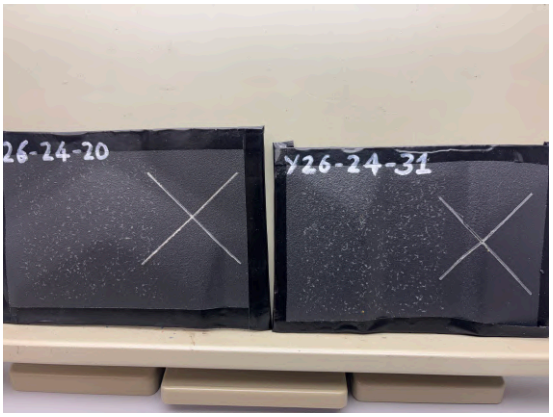

(c) Series 24, Y26-24-20 and Y26-24-31.

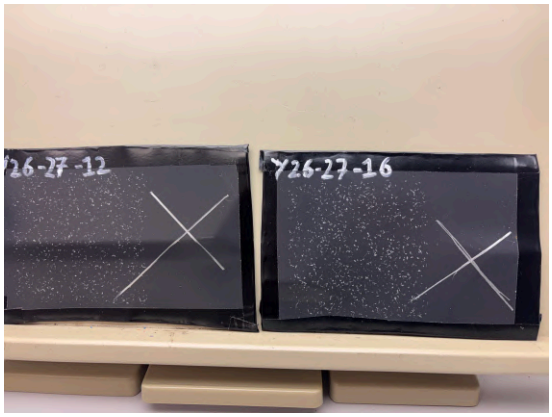

(d) Series 27, Y26-27-12 and Y26-27-16.

Figure 4.4.8: Wet-conditioned samples after high-pressure water-jet testing. All evaluated series are assigned rating 1 according to STD4234, with Series 23 showing discoloration in the exposed water-jet area but no rating-relevant delamination. The photographed panels are nominally 150 mm by 100 mm; cropping and masking mean that the full prepared-panel outline is not equally visible in every panel.

4.4.4 Knife-Edge Results Across Conditioning Routes

Knife-edge adhesion was assessed after standard, wet, and PV1200 conditioning using STD2239. The knife-mark edge was mechanically challenged and rated from 0 to 3, with lower values indicating better adhesion. Table 4.4.6 summarizes the knife-edge results across the three conditioning routes. The table is limited to the ratings; the main trend is described in the following paragraph.

Table 4.4.6: STD2239 knife-edge ratings across the relevant conditioning routes.

Conditioning route	*Series 22*	*Series 23*	*Series 24*	*Series 27*
Standard	0	0	1	1
Wet	0	0	1	1
PV1200, 20 cycles	0	0	2	1

Series 22 and *Series 23* remained at rating 0 in all routes. *Series 27* remained at rating 1. *Series 24* changed from rating 1 after standard and wet conditioning to rating 2 after PV1200, indicating increased local top-layer sensitivity after cyclic environmental exposure rather than complete coating-system loss.

4.4.5 Cross-Cut Results Across Conditioning Routes

Cross-cut adhesion was evaluated after standard, wet, and PV1200 conditioning according to ISO 2409. Table 4.4.7 summarizes the cross-cut results across the three conditioning routes. The table reports only the assigned classes, while the observed difference between systems is described in the text below.

Table 4.4.7: ISO 2409 cross-cut classes across the relevant conditioning routes.

Conditioning route	*Series 22*	*Series 23*	*Series 24*	*Series 27*
Standard	0	0	0	0
Wet	0	0	0	0
PV1200, 20 cycles	0	0	1	0

The standard- and wet-conditioned samples were class 0 for every series. After PV1200, *Series 22*, *Series 23*, and *Series 27* remained class 0, while *Series 24* was class 1 because of small lattice-square detachment. The thin *Series 22* and *Series 23* films were more difficult to cut cleanly, but the successfully formed lattice areas showed no detached squares. The *Series 24* wet-conditioned result had a borderline visual appearance but remained below class 1, while the PV1200-conditioned *Series 24* result showed sufficient detachment for class 1.

4.4.6 Cupping Test

The ISO 1520-style cupping test was performed on available samples as a constrained comparative mechanical assessment. *Series 24* was the least resistant to imposed deformation in this comparison: it developed a sudden clear crack at 2.3 mm, while the other systems showed more gradual visible change before their selected endpoints. Table 4.4.8 summarizes the measured endpoints. Because the samples were not ideal flat panels, the values are used comparatively rather than as fully standard-equivalent coating properties. The trial sample Y26-22-73 was used only for equipment familiarization and is not included in the main four-series comparison.

The clear-damage endpoint ranking from this single-sample comparison is *Series 23*, *Series 22*, *Series 27*, and *Series 24*. *Series 24* behaved differently from the other systems: *Series 22*, *Series 23*, and *Series 27* showed more gradual whitening or small-crack development, while *Series 24* showed a comparatively sudden paint-system crack at a lower displacement. This supports the broader interpretation that *Series 24* can perform well on intact surfaces but can be locally sensitive once deformation exposes a vulnerable region.

Table 4.4.8: Cupping-test visible-damage endpoints for the evaluated samples. Values are indenter displacement readings at observed visual damage points.

Series	Sample	Early subtle change	Clear-damage endpoint	Observation summary
22	Y26-22-23	5.1 mm	8.4 mm	Tiny cracks or whitening first; clear visible mark at the endpoint
23	Y26-23-16	7.1 mm	8.8 mm	Whitening at indentation sides first; clear crack and slight sample tearing at endpoint
24	Y26-24-16	–	2.3 mm	Sudden clear crack; substrate visible beneath cracked coating
27	Y26-27-21	1.8 mm	3.9 mm	Very small whitening or tiny cracks first; first clearly visible crack at endpoint

(a) ERICHSEN cupping tester used for the constrained ISO 1520-style test.

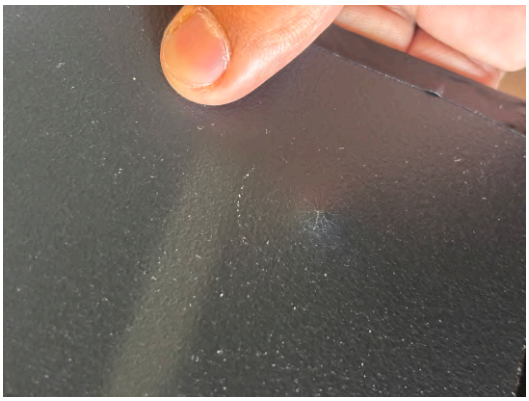

(b) Series 24 clear crack after cupping; preferred close-up evidence for Y26-24-16.

Figure 4.4.9: Cupping-test setup and Series 24 crack evidence.

4.4.7 Pendulum Hardness

Pendulum hardness was evaluated for the two powder-coated systems using the ISO 1522:2022 König damping-time method. *Series 22* and *Series 23* were not tested because the method was selected for comparing the thicker organic coating films rather than the thin inorganic zinc-nickel/passivation systems. Table 4.4.9 summarizes the valid readings.

Series 27 had a substantially longer mean damping time than *Series 24*, indicating a much harder and slower-damping powder-coating response. *Series 24* combined a short damping time with the sudden low-displacement crack observed in

Table 4.4.9: Comparative König pendulum damping times for the powder-coated systems. Longer damping time indicates a harder, slower-damping coating response under this method.

Series	Sample	Valid damping times	Mean	Interpretation
22	–	Not tested	–	Thin inorganic system; outside the selected comparison.
23	–	Not tested	–	Thin inorganic system; outside the selected comparison.
24	Y26-24-39	13 s, 10 s, 21 s, 16 s, 12 s and 19 s	15.2 s	Softer, faster-damping response.
27	Y26-27-09	158 s, 173 s and 167 s	166.0 s	Much harder, slower-damping response.

cupping, supporting a softer/fast-energy-dissipating response that can nevertheless fail locally in a brittle crack-type mode. Since ideal flat panels were unavailable, both systems were measured on selected stable regions and the values are treated as a comparative response rather than absolute flat-panel material constants.

4.4.8 Scratch Visibility Assessment

The DUR-O-Test result was interpreted using the project-specific first-normally-visible-scratch criterion described in Chapter 3. This comparative route was used because the applicable requirement framework does not define a scratch-test requirement for C3 components. *Series 27* was the most resistant to a normally visible scratch, requiring the 0–10 N spring at its maximum tested scale setting, corresponding to 10 N; *Series 24* ranked second, first becoming normally visible at 3 N using the 0–3 N spring at its maximum tested scale setting. *Series 22* and *Series 23* showed visible lines at every tested setting, so their thresholds lie at or below the lowest applied setting. Table 4.4.10 summarizes this ranking without assigning a compliance classification. The retained labelled result set confirmed the series-level thresholds; individual scratch sample IDs were not recoverable from the laboratory record and are therefore treated as a traceability limitation.

The ranking is therefore *Series 27*, *Series 24*, followed by *Series 22* and *Series 23* below the tested threshold. The thin metallic zinc-nickel/passivated surface character of *Series 22* and *Series 23* may contribute to the strong optical contrast of their scratch lines.

Table 4.4.10: Comparative DUR-O-Test scratch-visibility thresholds. Higher first-visible settings indicate greater resistance to a normally visible scratch under this project-specific route.

Series	First normally visible scratch	Observation and interpretation
22	At or below the lowest tested setting: 0–3 N spring at scale setting 150	Every tested scratch was visible; the threshold lies at or below the lowest tested setting.
23	At or below the lowest tested setting: 0–3 N spring at scale setting 150	Every tested scratch was visible; the threshold lies at or below the lowest tested setting.
24	3 N: 0–3 N spring at scale setting 300	First normally visible line occurred at the maximum setting of the 0–3 N spring.
27	10 N: 0–10 N spring at scale setting 300	First normally visible line required the maximum setting of the 0–10 N spring.

4.5 Corrosion Testing

Two cyclic corrosion exposure routes were used: VDA 233-102 testing through RISE with weekly inspections, and ACT1 testing through Cotec Labs. The VDA evaluation was separated by coating type because the inorganic zinc-nickel/passivation systems and the powder-painted systems were not judged by the same corrosion metric. *Series 22* and *Series 23* were evaluated primarily at the three-week VDA checkpoint using the metallic-coating appearance/protection rating framework, while *Series 24* and *Series 27* were evaluated after six weeks using painted-system scribe-creep measurements [21, 22, 23]. Cotec Labs performed the complementary four-week C3-IF ACT1 programs for *Series 22*/*Series 23* and six-week C3-PP ACT1 programs for *Series 24*/*Series 27*.

Table 4.5.11: VDA corrosion summary by coating-system evaluation route. Series 22/Series 23 use the inorganic-coating ISO 10289 rating route at the three-week checkpoint, while Series 24/Series 27 use the six-week painted-system spread-from-scribe route.

Series	Evaluation route	Reported result
22	Metallic-coating appearance/protection rating at three weeks	$R_{\mathrm{A}}7/R_{\mathrm{p}}10$
23	Metallic-coating appearance/protection rating at three weeks	Mainly $R_{\mathrm{A}}6/R_{\mathrm{p}}10$; one sample $R_{\mathrm{A}}7/R_{\mathrm{p}}10$
24	Painted-system scribe-creep measurement after six weeks	Maximum 1.0 mm
27	Painted-system scribe-creep measurement after six weeks	Maximum 1.5 mm

The VDA results therefore show different limiting observations for the two coating groups. In this thesis, red corrosion refers to reddish-brown rust products associated with corrosion of the steel substrate, in contrast to white corrosion products

from the zinc-nickel coating. *Series 22* met the applied $R_A \geq 7$ white-corrosion target and showed no visible red corrosion in the reviewed images, while *Series 23* was more affected in appearance because most samples were rated $R_A 6 / R_p 10$. For the painted systems, both *Series 24* and *Series 27* showed limited propagation from the scribe after six weeks, with maximum spread values of 1.0 mm and 1.5 mm, respectively.

The received ACT1 reports for *Series 22* and *Series 23* indicate 0 mm propagation from scribe through the recorded inspection points, but the report-level interpretation differs between the two systems. *Series 22* should be read as a majority-acceptable result with a local caveat: seven of the nine exposed samples remained without visible steel-rust spots, while samples Y26-22-18 and Y26-22-24 showed red corrosion spots / $R_p < 10$. *Series 23* remains the weaker inorganic ACT1 case because of lower R_A appearance ratings, especially the week-3 white-corrosion concern around Y26-23-21, even though the later R_p check can be fulfilled. The ACT1 result therefore reinforces the distinction between propagation-from-scribe behaviour and broader appearance/protection ratings for the inorganic systems.

The completed six-week ACT1 programs for *Series 24* and *Series 27* produced different report-level outcomes despite strong direct corrosion rows for both systems. *Series 24* showed no visible rusting through six weeks, corresponding to ISO 4628-3 rust grade Ri 0, and showed 0 mm propagation from scribe, while the post-ACT1 cross-cut, water-jet, knife, and stone-chip rows met the stated requirements. Its verification report nevertheless classified the overall requirements as not fulfilled because several coating-thickness values exceeded the listed 200 µm open-surface limit and cracks were recorded on samples Y26-24-30 and Y26-24-32. *Series 27* fulfilled the report requirements: all general-corrosion observations corresponded to ISO 4628-3 rust grade Ri 0, including the corrected classification of Y26-27-20, and the six-week scribe-propagation values of 2.0 mm, 1.9 mm, and 1.6 mm remained below the 3.5 mm C3 limit. Its post-ACT1 adhesion rows also met the stated requirements. The *Series 24* report-level nonfulfilment is therefore distinguished from a direct corrosion failure, whereas *Series 27* provides the cleanest powder-painted ACT1 outcome.

4.6 Chemical Resistance

Chemical resistance testing was completed for one sample from each series using the sponge spotting method described in Chapter 3. Across the four evaluated samples, no blistering, cracking, flaking, rusting, corrosion, delamination, or rated appearance change was visible. Using ISO 4628-1 as the visual reporting framework, all evaluated series were assigned rating 0 for visible coating defects and intensity of appearance change [25]. The only additional observation was possible extremely slight cloudiness on *Series 23*, which is retained as a qualitative note rather than a rated defect.

Table 4.6.12: Chemical resistance observations after project-specific sponge spotting. ISO 4628-1 is used only as the visual rating framework for the observed coating condition; the exposure method itself is a project-specific adaptation guided by STD4113.

Series	Sample	ISO 4628-1 visual rating	Additional observation
22	Y26-22-12	0	No additional observation
23	Y26-23-25	0	Possible extremely slight cloudiness noted qualitatively
24	Y26-24-23	0	No additional observation
27	Y26-27-18	0	No additional observation

4.7 UV/Weathering Exposure

The UV/weathering results are reported in three stages: baseline condition, the 400 h checkpoint, and the final cleaned, unpolished condition after approximately 853 h. Colour changes are reported using CIELAB coordinates, where L^* describes lightness, a^* describes the green-red axis, and b^* describes the blue-yellow axis.

4.7.1 Baseline Condition

Baseline colour was measured for all 12 UV/weathering samples, with three left–centre–right readings per sample. Table 4.7.13 reports the resulting baseline series means. Baseline gloss was recorded on one representative UV sample and one flatter reference sample per series because the cut UV panels were not equally suitable for stable glossmeter seating. Table 4.7.14 reports these baseline gloss readings together with auxiliary instrument outputs.

Table 4.7.13: Baseline CIELAB colour summary for UV/weathering samples before exposure. Values are averages of the three UV samples in each series, with each sample measured at left, centre, and right positions.

Series	Samples	Mean L^*	Mean a^*	Mean b^*
22	Y26-22-1–Y26-22-3	69.07	-0.27	1.61
23	Y26-23-1–Y26-23-3	24.80	1.12	0.94
24	Y26-24-1–Y26-24-3	29.58	-0.18	-1.06
27	Y26-27-1–Y26-27-3	33.10	-0.21	-2.02

The 20°, 60°, and 85° columns refer to the ISO 2813 glossmeter measurement geometries. The 60° geometry is used as the primary gloss comparison for *Series 22*, *Series 23*, and *Series 27*. *Series 24* is a very low-gloss surface, so the 85° geometry provides the more sensitive matt-surface comparison according to ISO 2813 [27]. The unusually low 85° baseline value for Y26-27-3 is retained with caution because it differs strongly from the flatter *Series 27* reference sample.

Table 4.7.14: Baseline gloss and auxiliary appearance readings for representative UV samples and flatter reference samples before UV/weathering exposure. Gloss is reported in gloss units (GU) at the ISO 2813 geometries. DOI, logHaze, and RSpec are retained as instrument outputs but are secondary to the gloss values in the present analysis.

Role	Sample	Series	20°	60°	85°	DOI	logHaze	RSpec
Reference	Y26-22-28	22	9.9	33.5	27.8	0.8	451	1.5
UV sample	Y26-22-3	22	10.0	37.8	29.0	2.0	454	1.5
Reference	Y26-23-9	23	4.9	28.2	53.0	1.5	222	0.7
UV sample	Y26-23-1	23	4.0	23.7	43.4	1.1	213	0.6
Reference	Y26-24-42	24	0.3	3.8	1.3	0.0	19.5	0.1
UV sample	Y26-24-3	24	0.3	3.4	2.8	0.0	14.3	0.1
Reference	Y26-27-28	27	21.1	60.2	86.7	3.7	439	2.9
UV sample	Y26-27-3	27	20.7	61.9	3.2	4.1	432	2.9

4.7.2 Intermediate Response at 400 h

Table 4.7.15 summarizes the intermediate CIELAB means after 400 h. The delta values are calculated relative to the baseline series means in Table 4.7.13; for example, ΔL^* is the 400 h mean L^* value minus the baseline mean L^* value.

Table 4.7.15: Intermediate CIELAB colour summary after 400 h of UV/weathering exposure. Means include the three UV samples in each series and three left–centre–right readings per sample. The deltas are relative to the corresponding baseline series means in Table 4.7.13.

Series	Mean L^*	Mean a^*	Mean b^*	ΔL^*	Δa^*	Δb^*
22	71.62	0.14	2.63	+2.55	+0.42	+1.02
23	17.00	2.59	4.19	-7.79	+1.47	+3.25
24	30.62	-0.28	-1.37	+1.04	-0.10	-0.31
27	33.67	-0.28	-2.18	+0.57	-0.06	-0.16

Series 23 showed the clearest intermediate colour response: mean L^* decreased from 24.80 to 17.00, while a^* and b^* increased. This agrees with the visible discoloration at the checkpoint. *Series 22* became lighter on average, whereas *Series 24* and *Series 27* showed comparatively small coordinate changes.

The matched-sample values in Table 4.7.16 provide the primary intermediate gloss comparison because equivalent baseline measurements were not available for every panel.

Table 4.7.16: Matched-sample gloss comparison from baseline to the 400 h UV/weathering checkpoint. Only UV samples with both baseline and 400 h gloss readings are included. Gloss deltas are reported in GU.

Sample	Series	Δ 20°	Δ 60°	Δ 85°	Intermediate note
Y26-22-3	22	+1.6	+14.6	+1.1	Same UV sample; 60° gloss increases at the checkpoint.
Y26-23-1	23	-2.7	-11.0	-3.8	Same UV sample; gloss decreases at all stored geometries.
Y26-24-3	24	0.0	-0.4	-1.6	Same UV sample; the surface remains very low-gloss.
Y26-27-3	27	-6.4	-7.4	+0.1	Same UV sample; interpretation remains cautious because flatness and baseline 85° behaviour are uncertain.

4.7.3 Final Response after Approximately 853 h

At final removal, *Series 22* and *Series 24* showed no obvious visual colour change in the cleaned, unpolished condition. *Series 23* changed from black toward a reddish-black or bronze appearance, with a possible iridescent effect. *Series 27* retained localized hazy spots after washing and drying. Table 4.7.17 summarizes the final CIELAB means after approximately 853 h. The delta values are calculated relative to the baseline series means in Table 4.7.13; therefore positive values indicate an increase from baseline and negative values indicate a decrease from baseline.

Table 4.7.17: Final cleaned, unpolished CIELAB colour summary after approximately 853 h of UV/weathering exposure. Means include the three UV samples in each series and three left–centre–right readings per sample. The deltas are relative to the corresponding baseline series means in Table 4.7.13.

Series	Mean L^*	Mean a^*	Mean b^*	ΔL^*	Δa^*	Δb^*
22	72.45	0.34	3.79	+3.38	+0.61	+2.18
23	23.90	2.08	2.90	-0.90	+0.96	+1.96
24	30.41	-0.29	-1.36	+0.83	-0.11	-0.30
27	33.76	-0.29	-2.11	+0.66	-0.08	-0.09

STD4113 Table 17 is used here as the gloss-permanence framework for artificial UV exposure [9]. The comparison is made before polishing, using the same UV samples that had baseline gloss readings. For *Series 22*, *Series 23*, and *Series 27*, the 60° geometry is used as the primary comparison. For *Series 24*, the very low 60° gloss means that 85° is more sensitive for matt-surface differentiation according to ISO 2813, but the small absolute gloss values make percentage changes sensitive to measurement uncertainty [27]. Table 4.7.18 summarizes the matched-

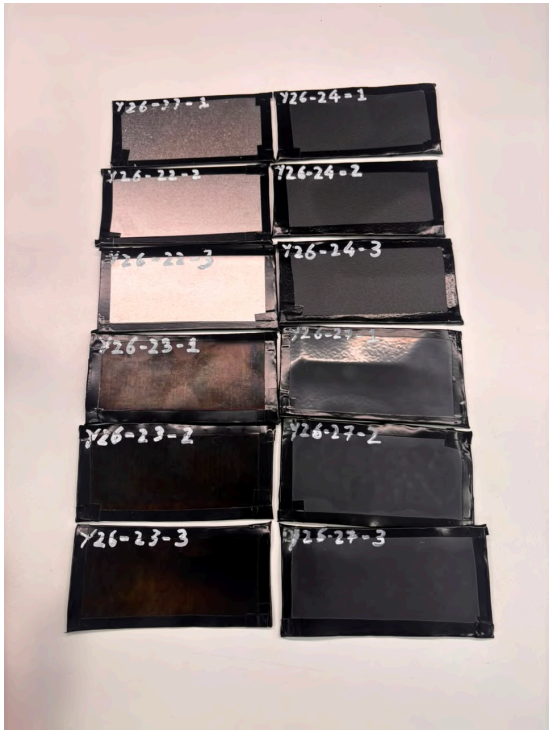

(a) All UV/weathering samples after final removal.

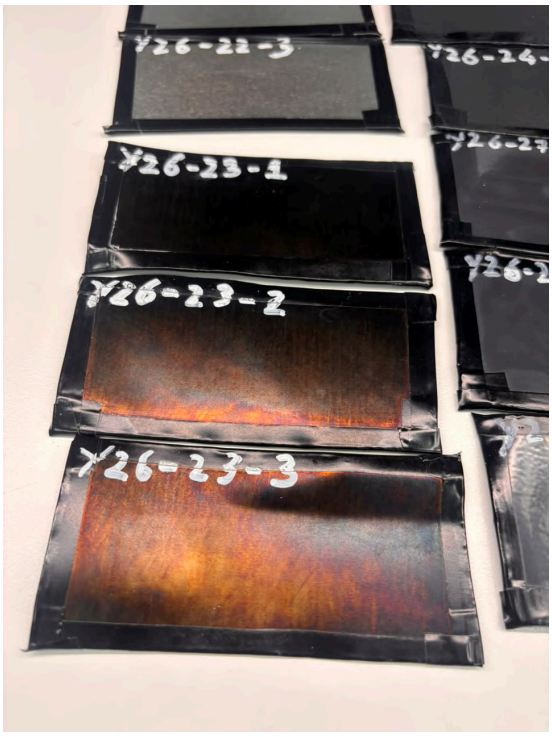

(b) Series 23 angled-light image showing reddish/bronze discoloration.

(c) Series 27 image showing localized hazy spotting.

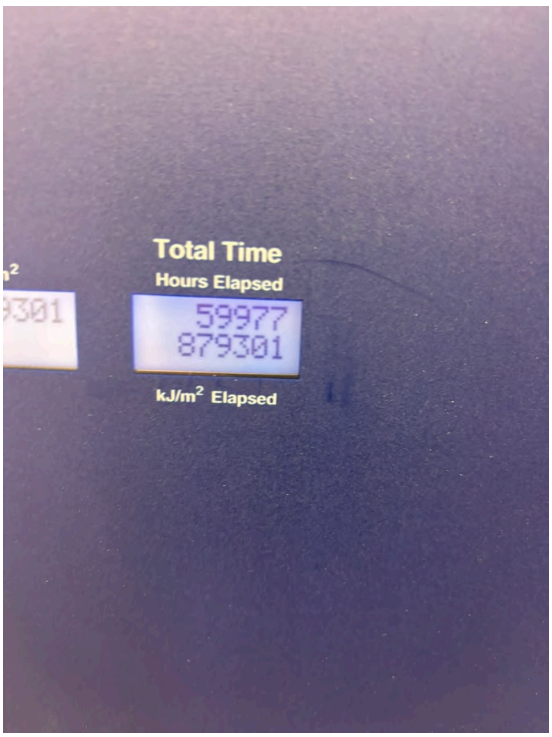

(d) Chamber display at final removal, showing 59977 h total elapsed.

Figure 4.7.10: Final UV/weathering evidence after approximately 853 h of counted chamber exposure. The UV/weathering samples were approximately 50 mm by 100 mm; the close-up panels show selected regions from these samples. Series 23 shows the clearest colour change, while Series 27 shows localized hazy spotting that is not strongly captured by the series-mean CIELAB values.

sample gloss change.

Table 4.7.18: Matched-sample gloss permanence comparison from baseline to the final cleaned, unpolished UV/weathering condition. Positive gloss-reduction values indicate gloss loss. Negative values indicate that the final measured gloss was higher than the baseline reading.

Sample	Series	Geometry	Baseline GU	Final GU	Interpretation note
Y26-22-3	22	60°	37.8	57.9	No gloss loss; final measured gloss increased.
Y26-23-1	23	60°	23.7	18.3	22.8 % gloss reduction; main gloss-permanence concern but still below the likely C3 artificial-UV limit.
Y26-24-3	24	60°	3.4	2.9	14.7 % reduction by 60°; absolute change is only 0.5 GU.
Y26-24-3	24	85°	2.8	1.6	42.9 % reduction by the matt-sensitive geometry; interpret cautiously because the absolute change is only 1.2 GU.
Y26-27-3	27	60°	61.9	55.5	10.3 % gloss reduction; moderate loss by the primary geometry.

The final gloss comparison indicates no gloss-loss concern for *Series 22*. *Series 23* had the largest meaningful 60° gloss reduction. *Series 24* remained very low-gloss; although its percentage reduction appears large at 85°, the absolute change was only 1.2 GU. *Series 27* showed moderate 60° gloss loss together with visible haze.

STD4113 Table 18 provides the colour-permanence framework, with ISO 3668 supplying the visual comparison language [9, 28]. The measurements represent the cleaned, unpolished condition. *Series 22* and *Series 24* are low-concern cases. *Series 23* is the main colour-permanence concern because the visible reddish/bronze shift is stronger than the series-mean CIELAB change alone suggests. *Series 27* changed little in average colour coordinates, but its persistent haze remains a separate appearance concern.

4.8 Comparative Performance Summary

The comparative summary combines the result packages into the multifunctional structure described in Section 3.12. Table 4.8.19 summarizes coating build and key evidence from the completed test routes.

Overall, *Series 24* remains the strongest protective reference but is least favourable for electrical grounding in the dry-circuit comparison. *Series 22* has the strongest conductivity response and the cleaner VDA appearance rating among the inorganic candidates, with the ACT1 concern treated as visible steel-rust spots on two of nine samples rather than a broad majority failure. *Series 23* is also conductive, and the corrected screening values show a smaller gap to *Series 22* than the first run suggested, but its stronger contact sensitivity, corrosion-appearance

Table 4.8.19: Performance comparison matrix based on the thesis results. The entries separate direct experimental evidence from external corrosion-report evidence where applicable.

Series	Coating build	Key evidence
22	Thin zinc/nickel-rich inorganic system; mean thickness approx. 13.2 µm.	Lowest dry-circuit resistance, approx. 0.11 Ω over 50 mm. Stone-chip grade 2 in PV1200, wet, and freezer routes; water-jet rating 1; cross-cut and knife-edge rating 0 in PV1200/wet tests. Chemical rating 0; VDA $R_{\mathrm{A}}7/R_{\mathrm{p}}10$ at three weeks; ACT1 majority acceptable with visible steel-rust spots on two of nine samples.
23	Thin zinc/nickel-rich inorganic system; mean thickness approx. 8.9 µm.	Measurable dry-circuit resistance, approx. 0.20 Ω over 50 mm. Stone-chip grade 2 in PV1200, wet, and freezer routes; water-jet rating 1 with discoloration note; cross-cut and knife-edge rating 0 in PV1200/wet tests. Chemical rating 0 with possible slight cloudiness; VDA mainly $R_{\mathrm{A}}6/R_{\mathrm{p}}10$; largest UV colour/gloss concern.
24	Thick reference powder system; approx. 201.0 µm.	No measurable value under the dry-circuit setup. Strong stone-chip result: grade 1 after PV1200 and wet conditioning, grade 2 after freezer; water-jet rating 1; PV1200 knife-edge rating 2; DSC T_{g} mean 70.7 °C. Chemical rating 0; VDA spread from scribe up to 1.0 mm; ACT1 no visible rusting, corresponding to ISO 4628-3 rust grade Ri 0, and 0 mm scribe propagation, but report-level nonfulfilment due to thickness and cracking notes.
27	Intermediate powder/organic system with a visibly non-uniform interface; approx. 80.9 µm.	No measurable value under the dry-circuit setup. Stone-chip grade 2 in PV1200, wet, and freezer routes; water-jet rating 1; cross-cut rating 0; knife-edge rating 1; DSC T_{g} mean 77.0 °C. Chemical rating 0; VDA spread/blistering up to 1.5 mm; ACT1 requirements fulfilled with no visible rusting and scribe propagation below 3.5 mm; moderate UV gloss loss and visible haze.

response, and UV/weathering concerns make it less favourable overall. *Series 27* remains an intermediate protective candidate because it combines a thinner coating build than *Series 24* with generally acceptable adhesion and environmental results, but the dry-circuit conductivity result does not support it as a conductive replacement for the inorganic systems.

5 Discussion

5.1 Interpretation of Coating-System Performance

The thesis is framed around a multifunctional trade-off rather than a single-property optimization. A surface-treatment system for the battery enclosure lid must provide sufficient electrical conductivity while retaining corrosion resistance, adhesion, mechanical durability, chemical resistance, and weathering resistance. The reference system, *Series 24*, was protective and mechanically robust in several evaluations, but its thickness and insulating powder-coating structure produced no stable measurable value in the dry-circuit comparison. The thin zinc-nickel/passivation systems, *Series 22* and *Series 23*, provided the clearer electrical response. The repeat screening favoured *Series 22* over *Series 23*, although the difference was smaller than the first run suggested; the result therefore supports a comparative ranking rather than a large absolute separation.

Series 27 represents an intermediate coating architecture: thinner than the *Series 24* reference system but still a powder-coating system with an ED primer layer. Its dry-circuit result does not support it as a conductive alternative to *Series 22* or *Series 23*. However, its fulfilled ACT1 requirements, no visible rusting according to ISO 4628-3 rust grade Ri 0, acceptable scribe propagation, and generally sound adhesion response make it the strongest powder-coated compromise within the tested scope. *Series 24* also retained strong direct ACT1 corrosion indicators, but its excessive-thickness rows and cracking observations demonstrate that protective performance cannot be separated from coating-build control.

The DSC comparison provides an additional thermal distinction between the powder coatings. *Series 27* had a mean T_g of 77.0 °C, compared with 70.7 °C for *Series 24*. *Series 27* therefore remained below its glass-transition-related softening region to a higher temperature and showed better resistance to thermally induced softening in this specific material comparison. This advantage is limited to the measured cured-coating thermal response and does not override the conductivity, corrosion, adhesion, or mechanical evidence.

5.2 Methodological Strengths and Limitations

A strength of the project is that the coating systems are evaluated using several complementary methods rather than only conductivity measurements. Thickness, adhesion, corrosion, weathering, chemical resistance, mechanical behavior, and microscopy together provide a broader basis for assessing coating suitability.

The main limitations are connected to the industrial project setting, sample availability, and external testing. Conductivity was measured using a comparative dry-circuit screening route rather than an assembled frame/gasket/bolt interface. The dry-circuit principle is relevant to Scania electrical-conductivity practice, including STD4472 for electrically functional fastener joints, but the thesis setup was a coupon-level adaptation rather than the full fastener-joint procedure. The Keithley 2010 was used in four-wire resistance mode, which reduces the influence of lead resistance, but the handheld probe setup still includes the probe-to-sample contact effect because the probes form two effective surface contact points. This is suitable for comparing the supplied surface treatments, but it does not replace contact-resistance validation in the final bolted configuration and should not be compared directly with milliohm-level assembled equipotential-bonding requirements. Sample availability limited the number of replicates in some mechanical tests. The ACT1 interpretation also depends partly on verification reports and observations produced outside the author's direct experimental control.

The SEM/EDS results strengthen the coating-stack interpretation compared with the earlier optical microscopy package. They confirm that the substrate is steel, support the zinc/nickel-rich layer interpretation for *Series 22* and *Series 23*, and show a zinc-rich substrate-side layer in the powder-coated *Series 24* system. The thesis therefore treats SEM/EDS as the primary microscopy evidence, while optical microscopy is retained as supporting context. This avoids over-interpreting local optical annotations from cold-mounted specimens.

The microscopy results still introduce a preparation-related limitation. The first optical cross-section samples were selected from unconditioned Standard Testing panels, so they are useful as baseline layer-structure observations. However, cutting and cold mounting caused local damage, particularly in *Series 24*. The earlier *Series 24* optical recheck suggested that a visually unclear intermediate feature was local rather than continuous. SEM/EDS improves the chemical interpretation of the layer stack, but local preparation sensitivity and exposed-edge damage remain relevant when discussing *Series 24* behavior.

The cupping result points in the same direction. *Series 24* showed a clear crack at a lower displacement than the other tested systems, while *Series 22*, *Series 23*, and *Series 27* showed more gradual visible change. This does not contradict the strong stone-chip and water-jet performance of *Series 24*; instead, it suggests that the reference coating may perform well under intact-surface adhesion and impact screening but can fracture more abruptly under imposed deformation or where preparation exposes a vulnerable interface.

The pendulum-hardness comparison adds a complementary coating-response measure for the powder systems. *Series 27* had a mean König damping time of

166.0 s, compared with 15.2 s for *Series 24*, indicating a much harder and slower-damping *Series 27* response. *Series 24* therefore combines strong intact-system protection in several routes with a softer/fast-damping pendulum response and a sudden cupping crack. Because the available panels were not ideally flat, the pendulum values are comparative rather than absolute material constants.

The constrained scratch assessment adds a different mechanical comparison. *Series 27* was the most resistant to a normally visible scratch, requiring the highest first-visible setting at 10 N; *Series 24* ranked second at 3 N. *Series 22* and *Series 23* showed visible lines at all tested settings. This may partly reflect the strong optical contrast of scratches on their thin metallic/passivated surfaces rather than only lower mechanical scratch resistance. The applicable requirement framework defines scratch-test requirements for A1, A2, B1, B2, C1, and C2 components, but not for C3 components. A comparative first-visible-scratch criterion was therefore used to distinguish the four systems without assigning a C3 compliance result or treating the values as a direct hardness ranking across dissimilar coating architectures.

5.3 Industrial Relevance

The results support TRATON's continued evaluation of conductive surface-treatment systems for electrified vehicle battery enclosure applications. A successful candidate should reduce the need for local coating removal to establish electrical contact while preserving protective performance in automotive environments. The conductivity screening showed that the zinc-nickel/passivation systems provided measurable electrical pathways that were absent in the powder-coated systems under the applied low-energy route. *Series 22* is consequently the strongest conductive implementation candidate within the tested scope, but its two local ACT1 observations of visible steel-rust spots require explicit corrosion-risk control and assembled-interface validation before production selection.

5.4 Societal and Ethical Reflection

The project contributes to the sustainability of electrified heavy vehicles by supporting battery enclosure components that retain both protective and electrical functions over their intended service life. A durable coating can reduce maintenance, premature component replacement, associated material demand, and waste. A conductive as-coated surface may also reduce local laser removal around electrical contact points, thereby avoiding an additional manufacturing operation and limiting deliberately exposed regions that could become corrosion initiation sites. These benefits depend on selecting a system that remains sufficiently protective; replacing a durable coating solely to improve conductivity could instead shorten service life and shift environmental burdens elsewhere.

The broader societal and ethical responsibility is therefore to evaluate the complete performance balance rather than promote a single favourable measurement. Coating selection should consider energy and water use in surface treatment, chemical handling, worker safety, supplier feasibility, repairability, and end-of-life implications alongside technical performance. Transparent reporting of uncertainty is particularly important in an industrial thesis because an overstated

recommendation could influence component reliability and resource use. The work must also balance industrial confidentiality with enough methodological clarity for academic scrutiny and responsible engineering judgement.

5.5 Use of Generative AI

Generative AI tools were used during thesis preparation to organize project context, structure draft text from the author's notes, support language revision, assist with LaTeX editing, and prepare author-reviewed conceptual or redrawn schematic figures where explicitly stated in the relevant figure captions. All experimental decisions, measurements, interpretations, source selection, technical verification, and final editorial decisions remained the responsibility of the author. The author reviewed and edited the resulting text and figures before inclusion.

6 Conclusions

This chapter combines the principal conclusions with the resulting coating-system recommendation. The central outcome is not a universally superior coating, but a clear distinction between the best conductive candidate and the strongest protective alternatives.

6.1 Conclusions and Recommendation

- ***Series 22* is the recommended candidate when an electrically conductive as-coated surface is required.** It gave the lowest resistance in the dry-circuit screening and was less contact-sensitive than *Series 23*. The recommendation remains conditional because visible steel-rust spots, reported as red corrosion in the ACT1 assessment, occurred on two of nine samples; corrosion-risk control and validation in the assembled electrical interface are required before implementation.
- ***Series 24* should remain the protective reference system.** It combined strong adhesion and low direct corrosion propagation with the established thick protective architecture, but no stable resistance value was measurable under the applied low-voltage/low-current conditions. Its ACT1 report-level nonfulfilment reflected coating-thickness nonconformance and associated cracking observations rather than failure of the direct corrosion indicators, showing that its performance depends on coating-build control. It is therefore suitable as the protection benchmark, but it does not solve the grounding-contact problem without local coating removal or another contact strategy.
- ***Series 27* is the strongest powder-coated option within the tested scope where conductivity is not required.** It fulfilled the ACT1 requirements, retained sound adhesion, showed the highest scratch-visibility threshold, and had both a much longer König damping time and a higher mean T_g than *Series 24*. These results indicate a harder coating response and better resistance to glass-transition-related softening. However, its lack of a stable dry-circuit resistance value excludes it as a conductive replacement for *Series 22*.

- ***Series 23* is less favourable than *Series 22* as the conductive alternative.** It remained electrically conductive, but showed higher and more contact-dependent resistance, the weakest inorganic ACT1 appearance response, and the clearest UV-related colour change. Its thinner coating build did not produce a compensating advantage in the complete performance comparison.
- **The mechanical results distinguish coating response rather than identify one universally toughest system.** *Series 24* performed strongly in several intact-surface adhesion and impact evaluations but cracked abruptly at a lower cupping displacement and showed a short pendulum damping time. *Series 27* showed the strongest scratch and pendulum response, while the thin metallic *Series 22* and *Series 23* surfaces were visibly marked at every tested scratch setting.
- **The microscopy supports the functional interpretation of the systems.** SEM/EDS confirmed the steel substrate, thin zinc/nickel-rich architectures in *Series 22* and *Series 23*, and a zinc-rich substrate-side region beneath the *Series 24* powder coating. Together with the large measured thickness differences, this explains why the thin inorganic systems favour electrical continuity while the thicker organic systems favour barrier protection.
- **The overall selection must remain multifunctional.** Conductivity alone would favour *Series 22*, whereas protection-focused evidence favours *Series 24* or *Series 27*. The appropriate choice therefore depends on whether the application requires conduction through the as-coated surface and on whether the remaining corrosion risk can be controlled.

6.2 Future Work

The next qualification step should test *Series 22* in the actual frame/gasket/bolt interface and repeat the electrical measurement after representative environmental exposure. Flatter panels and larger replicate sets would reduce uncertainty in the mechanical comparisons. Additional work could include quantitative EDS composition export and a defined assembled-interface acceptance criterion for grounding performance.

Bibliography

[1] "Advances in Corrosion Protection Coatings: A Comprehensive Review". In: *International Journal of Corrosion and Scale Inhibition* 12.4 (2023). DOI: 10.17675/2305-6894-2023-12-4-6.

[2] S. Syed Azim, A. Satheesh, K. K. Ramu, et al. "Studies on Graphite Based Conductive Paint Coatings". In: *Progress in Organic Coatings* 55.1 (2006), pp. 1–4. DOI: 10.1016/j.porgcoat.2005.09.001.

[3] Samira Naghdi, Kyong Yop Rhee, David Hui, et al. "A Review of Conductive Metal Nanomaterials as Conductive, Transparent, and Flexible Coatings, Thin Films, and Conductive Fillers: Different Deposition Methods and Applications". In: *Coatings* 8.8 (2018), p. 278. DOI: 10.3390/coatings8080278.

[4] M. R. Lambert, R. G. Hart, and H. E. Townsend. *Corrosion Mechanism of Zn-Ni Alloy Electrodeposited Coatings*. SAE Technical Paper 831817. SAE International, 1983.

[5] Tingyi Chen, Yaqi Ma, Qiming Huang, et al. "Preparation and Characterization of High Electrical Conductivity and Corrosion Resistant Black Passivation Film on Zn-Ni Alloy Coating of AA2024 Substrates". In: *Journal of Alloys and Compounds* 1051 (2026), p. 185976. DOI: 10.1016/j.jallcom.2026.185976.

[6] Yao Sun, Ha-Da Bao, Zhao-Xia Guo, et al. "Modeling of the Electrical Percolation of Mixed Carbon Fillers in Polymer-Based Composites". In: *Macromolecules* 42.1 (2009), pp. 459–463. DOI: 10.1021/ma8023188.

[7] D. D. L. Chung. "Materials for Electromagnetic Interference Shielding". In: *Materials Chemistry and Physics* 255 (2020), p. 123587. DOI: 10.1016/j.matchemphys.2020.123587.

[8] Luca Savarino. "Epoxy-CNTs Composite Coatings for Conductive and Anticorrosive Applications". In: (2017). Master's thesis, Politecnico di Milano.

[9] Scania CV AB. *STD4113: Organic Surface Treatment - Painting of Metals - Requirements*. Revision 19. Internal Scania standard. Scania CV AB. May 14, 2025.

[10] International Organization for Standardization. *SS-EN ISO 2812-2:2018: Paints and Varnishes - Determination of Resistance to Liquids - Part 2: Water Immersion Method*. Edition 3. Used as supporting water-immersion context; STD4113 is the primary wet-conditioning reference in this thesis. SIS, Swedish Standards Institute. Dec. 19, 2018.

[11] Scania CV AB. *STD4111: Surface Treatment - Directives and Instructions*. Issue 17. Internal Scania standard. Scania CV AB. Feb. 24, 2021.

[12] Volkswagen AG. *PV 1200: Vehicle Parts, Testing of Resistance to Environmental Cycle Test (+80/-40) °C*. PV 1200: 2004-10. Volkswagen Group standard. Volkswagen AG. Oct. 2004.
[13] Scania CV AB. *STD4561: Stone Chip Resistance - Testing Method*. Issue 1. Internal Scania standard. Scania CV AB. June 1, 2018.
[14] Scania CV AB. *STD4234: Paints and Varnishes - Determination of Adhesion When Subjected to High-Pressure Spraying with Water*. Issue 3. Internal Scania standard. Scania CV AB. Feb. 21, 2020.
[15] International Organization for Standardization. *ISO 2409: Paints and Varnishes - Cross-Cut Test*. ISO 2409:2020. International standard. International Organization for Standardization. 2020.
[16] Scania CV AB. *STD2239: Surface Treatment - Testing Method - Assessment of Adhesion by Means of a Knife Edge*. Issue 7. Internal Scania standard. Scania CV AB. Mar. 24, 2021.
[17] International Organization for Standardization. *ISO 1520:2006: Paints and Varnishes - Cupping Test*. ISO 1520:2006. International standard. International Organization for Standardization. 2006.
[18] International Organization for Standardization. *ISO 1522:2022: Paints and Varnishes - Pendulum Damping Test*. ISO 1522:2022. International standard. International Organization for Standardization. 2022.
[19] Scania CV AB. *STD4472: Electrical Conductivity for Fasteners - Test Procedure*. Revision 4.1. Internal Scania standard. Scania CV AB. Jan. 29, 2024.
[20] Verband der Automobilindustrie. *VDA 233-102: Cyclic Corrosion Testing of Materials and Components in Automotive Construction*. VDA 233-102. Automotive cyclic corrosion test standard. Verband der Automobilindustrie. 2013.
[21] Scania CV AB. *STD4165: Surface Treatment - Requirements for Flake Coatings and Electroplated Zinc Coatings*. Issue 22. Internal Scania standard. Scania CV AB. Mar. 22, 2022.
[22] International Organization for Standardization. *ISO 10289: Methods for Corrosion Testing of Metallic and Other Inorganic Coatings on Metallic Substrates - Rating of Test Specimens and Manufactured Articles Subjected to Corrosion Tests*. ISO 10289:1999. International standard. International Organization for Standardization. 1999.
[23] Scania CV AB. *STD4271: Surface Treatment - Scribe Marks and Evaluating the Extent of Damage*. Revision 6. Internal Scania standard. Scania CV AB. Feb. 5, 2024.
[24] Scania CV AB. *STD4319: Accelerated Corrosion Test - Atmospheric Corrosion*. Issue 3. Internal Scania standard. Scania CV AB. Apr. 10, 2017.
[25] International Organization for Standardization. *ISO 4628-1:2016: Paints and Varnishes - Evaluation of Degradation of Coatings - Designation of Quantity and Size of Defects, and of Intensity of Uniform Changes in Appearance - Part 1: General Introduction and Designation System*. ISO 4628-1:2016. International standard. International Organization for Standardization. 2016.
[26] International Organization for Standardization. *SS-EN ISO 4892-2:2013: Plastics - Methods of Exposure to Laboratory Light Sources - Part 2: Xenon-Arc Lamps*. SS-EN ISO 4892-2:2013. Used as the local UV/weathering exposure-cycle reference. SIS, Swedish Standards Institute. Mar. 2013.
[27] International Organization for Standardization. *ISO 2813:2014: Paints and Varnishes - Determination of Gloss Value at 20 Degrees, 60 Degrees and 85 Degrees*. ISO 2813:2014. International standard. International Organization for Standardization. Oct. 1, 2014.

[28] International Organization for Standardization. *ISO 3668:1998: Paints and Varnishes - Visual Comparison of the Colour of Paints*. SS-EN ISO 3668:2001 / ISO 3668:1998. Used for visual colour comparison and colour-difference rating language. International Organization for Standardization. 1998.

Appendix A

Supplementary Experimental Material

A.1 DSC Thermal Analysis Result Graphs

Figure A.1.1 shows the complete DSC result-graph set for the powder-coated systems. The *Series 24* graph exports contain incorrect embedded software labels from the original export, but the source sample and values are corrected in the Results chapter table.

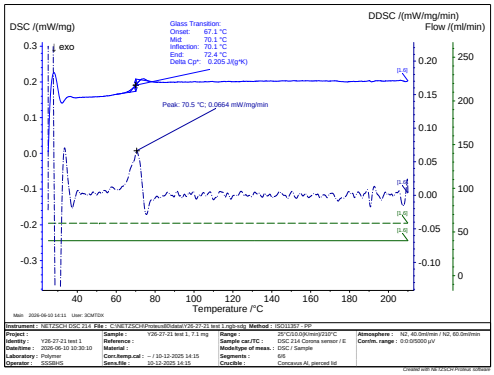

(a) Series 24, Test 1.

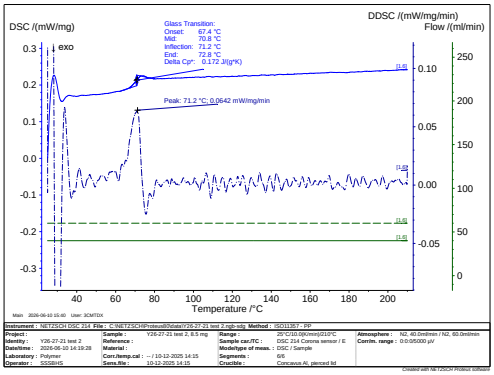

(b) Series 24, Test 2.

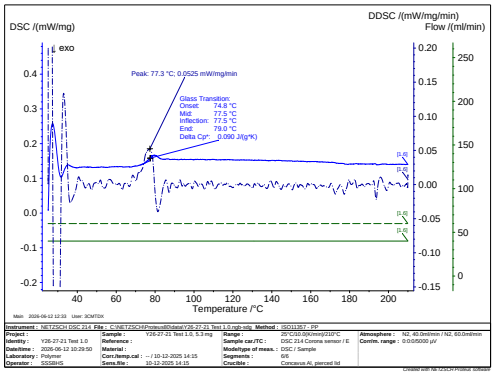

(c) Series 27, Test 1.

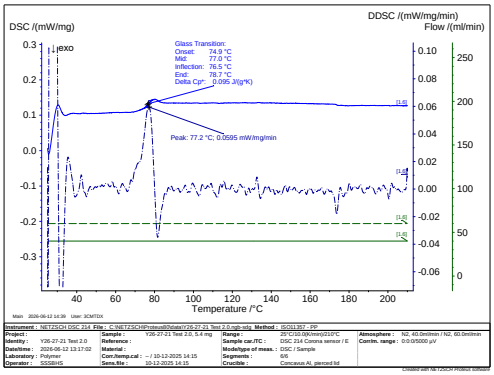

(d) Series 27, Test 2.

Figure A.1.1: Complete DSC result-graph set for powder-paint topcoat scrapings from Series 24 and Series 27.

A.2 Supporting Optical Cross-Section Images

The optical micrographs in Figure A.2.2 document the preliminary cross-section inspection that preceded SEM/EDS. They are retained as supporting morphology evidence rather than as the primary basis for layer identification because cutting, cold mounting, and local edge damage affected image interpretation.

(a) Series 22.

(b) Series 23, representative thin region.

(c) Series 24.

(d) Series 27.

Figure A.2.2: Supporting optical cross-section images at the preliminary inspection stage. Layer identity and final coating-stack interpretation are based primarily on the SEM/EDS evidence in Chapter 4.

A.3 Detailed Wet-Conditioned Adhesion Images

Figures A.3.3 and A.3.4 provide close views of the wet-conditioned cross-cut and knife-edge assessments. The numerical classifications remain the primary results in Chapter 4; these images allow the reader to inspect the coating edges underlying those ratings.

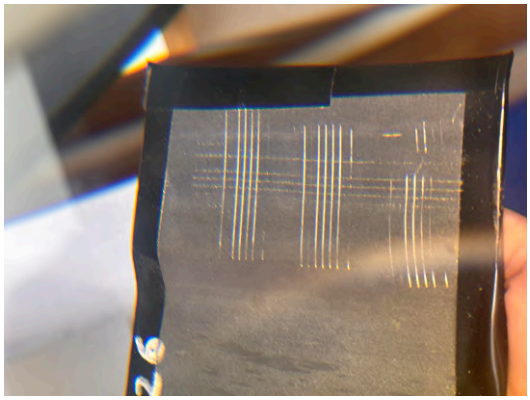

(a) Series 22.

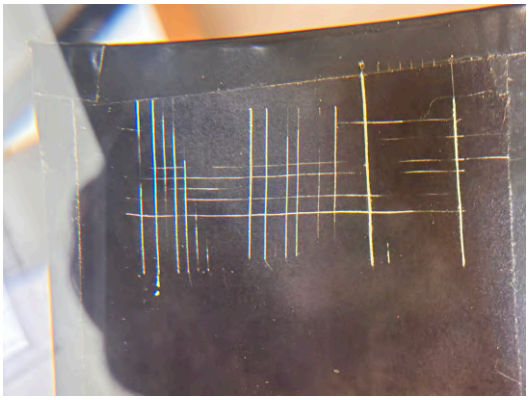

(b) Series 23.

(c) Series 24; overview including the cross-cut region.

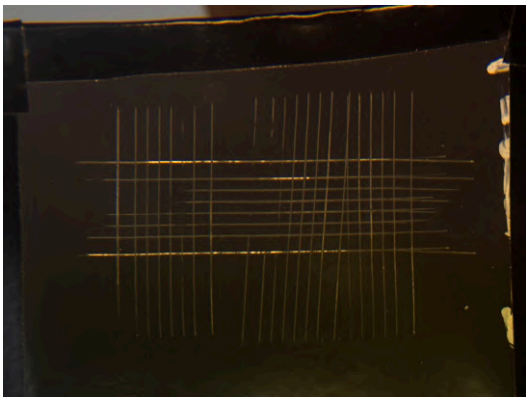

(d) Series 27.

Figure A.3.3: Wet-conditioned cross-cut result details for the four coating systems.

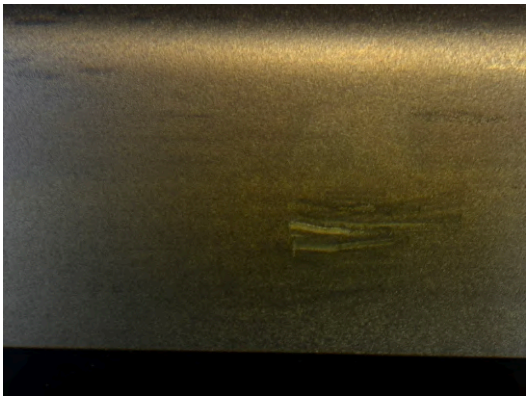

(a) Series 22.

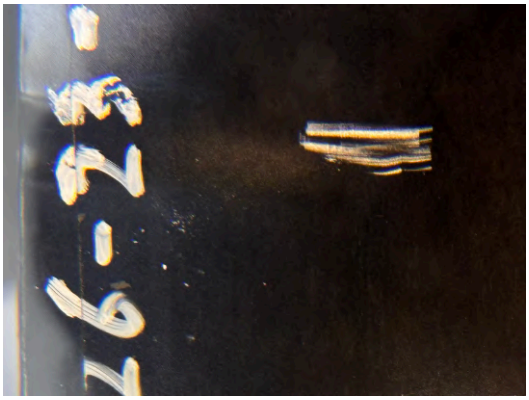

(b) Series 23.

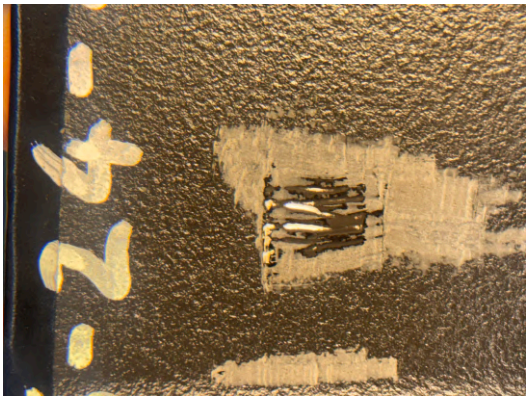

(c) Series 24.

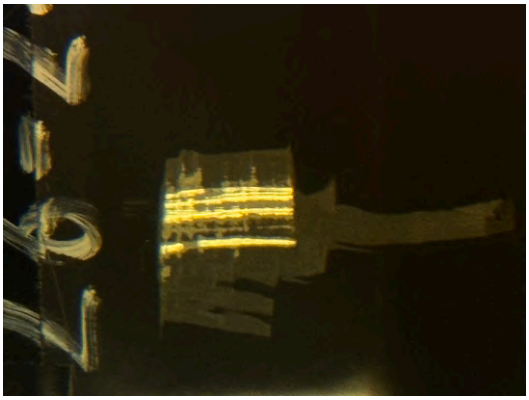

(d) Series 27.

Figure A.3.4: Wet-conditioned knife-edge result details after the marked coating edge was mechanically challenged.

KTH Royal Institute of Technology
Department of Materials Science and Engineering
Stockholm, Sweden

TRITA-ITM-EX 2026:196